This is to certify that the

thesis entitled

^{1}H NMR SPECTROSCOPIC STUDIES OF DINUCLEAR TRANSITION METAL CARBOXYLATE ADDUCTS OF DNA OLIGONUCLEOTIDES

presented by

Elizabeth Ursula Lozada Carrasco

has been accepted towards fulfillment
of the requirements for

Masters degree in Chemistry

Kevin R. Dunbar
Major professor

Date 7/28/98

^{1}H NMR SPECTROSCOPIC STUDIES OF DINUCLEAR TRANSITION METAL CARBOXYLATE ADDUCTS OF DNA OLIGONUCLEOTIDES

By

Elizabeth Ursula Lozada Carrasco

A THESIS

Submitted to
Michigan State University
in partial fulfillment of the requirements
for the degree of

MASTER OF SCIENCE

Department of Chemistry

1998

ABSTRACT

^{1}H NMR SPECTROSCOPIC STUDIES OF DINUCLEAR TRANSITION METAL CARBOXYLATE ADDUCTS OF DNA OLIGONUCLEOTIDES

By

Elizabeth Ursula Lozada Carrasco

Cisplatin, *cis*-$Pt(NH_3)_2Cl_2$, is in clinical use as an effective treatment for cancer. Its ability to bind covalently at the N7 position of guanine bases and form intrastrand cross-links with DNA is thought to be responsible for its biological activity. Similar metal-DNA interactions involving other transition metal compounds have been implicated, but none have been elucidated to date. Studies in our laboratories revealed an unprecedented bridging mode for dimetal carboxylate compounds of 9-ethylguanine and 9-ethyladenine involving the N7 and O6/N6 atoms. These results led us to investigate the type of interactions that occur with oligonucleotides. ^{1}H NMR spectroscopy was used to determine the solution structure of the duplex d(5'-CCTCTGGTCTCC-3') · d(5'-GGAGACCAGAGG-3') before and after reaction with $[Rh_2(O_2CCH_3)_2(CH_3CN)_6][BF_4]_2$. Differences in chemical shifts and intensities of the cross-peaks provided information about the perturbations of the oligonucleotide structure caused by covalent interactions with the metal at the GG sites of d(5'-CCTCTGGTCTCC-3').

TABLE OF CONTENTS

LIST OF TABLES

LIST OF FIGURES

LIST OF ABBREVIATIONS

cis-DDP	cis-Diamminedichloroplatinum (II)
RNA	Ribonucleic Acid
DNA	Deoxyribonucleic Acid
A	Adenine
C	Cytosine
G	Guanine
T	Thymine
p	Phosphate Group
HMG	High Mobility Group
SRY	Sex-determining Region Y protein
LEF-1	Lymphoid Enhancer Binding Factor 1
tsHMG	Murine Testis Specific High Mobility Group
trans-DDP	*trans*-Diamminedichloroplatinum
TBP	TATA Binding Protein
NMR	Nuclear Magnetic Resonance

JM216	Bis-Acetato-Ammine-Dichlorocyclohexylamine-platinum (IV)
NOE	Nuclear Overhauser Effects
FID	Free Induction Decay
M_o	Magnetization Vector
M_y	Transverse Magnetization Vector
B_o	Magnetic Field
B_1	External Magnetic Field
WATERGATE	Water Suppression by Gradient Tailored Excitation
NOESY	Nuclear Overhauser Effect Spectroscopy
W_1	First Order Transition
W_o	Zero Order Transition
W_2	Second Order Transition
S	Spin
T_1	Longitudinal Relaxation Time
T_2	Transverse Relaxation Time
τ_c	Correlation Time
τ_m	Mixing Time
t_1	Delay Time
t_2	Acquisition Time

F_1 ..... First Dimension

F_2 ..... Second Dimension

FID ..... Free Induction Decay

LP ..... Linear Prediction

TOCSY ..... Total Correlation Spectroscopy

ms ..... milliseconds

ns ..... nanoseconds

ps ..... picoseconds

2Q COSY ..... Two Quantum COSY

^1H ..... Proton

d ..... Deoxy

HPLC ..... High Performance Liquid Chromatography

nm ..... nanometers

min ..... minutes

mL ..... milliliters

g ..... grams

cm ..... centimeters

M ..... Molar

mM ..... millimolar

kDa ..... kiloDaltons

rpm ..... Revolutions per minute

ppm ..... parts per million

SA ..... Simulated Annealing

RMSD ..... Root Mean Square Deviation

MD ..... Molecular Dynamics

INTRODUCTION

Inorganic compounds have been used extensively as medicinal agents for centuries. Presently, metal compounds are in clinical use for the treatment of a number of diseases such as arthritis, hypertension, bacterial infections and cancer. Regarding the latter, a great deal of research has been conducted in the last 30 years due to the discovery that cisplatin and other related complexes exhibit remarkable efficacy in the chemotherapeutic treatment against several types of cancer.

Although the success of cisplatin as a chemotherapeutic agent has been well established and, indeed, it is currently in widespread use, its toxic side effects represent a considerable health risk for patients being treated with this drug. This disadvantage has provoked the search for new compounds with the same or higher activities but with lower toxicities than cisplatin.

The use of other transition metals as a possible alternative to platinum has been proposed in a number of studies over the years. In this dissertation, a structural study of the principal binding target of cisplatin, namely, the

intrastrand GpG cross-link is being investigated for dirhodium compounds. The main objective of this research is the elucidation of the mode of action of dimetal antitumor active compounds by understanding the structural distortions of DNA after metal binding has occurred. It is hoped that a better understanding of the DNA perturbations at the molecular level will lead to the discovery of new compounds that will satisfy the conditions necessary for inhibiting DNA replication in cancer cells.

Chapter 1

1. BACKGROUND

The history of the anticancer properties of the compound cisplatin, $PtCl_2(NH_3)_2$ or *cis*-DDP (Figure 1), dates back to 1965 when Professor Barnett Rosenberg and his research group observed filamentous growth of *E.coli* in experiments designed to study the effects of an electric field on the properties of these bacteria.[1] The bacterial cells, which normally divide very rapidly, grew up to 300 times their size without undergoing division. This observation was eventually recognized to be due to the presence of platinum-ammine complexes formed by *in situ* electrolysis of the Pt electrodes used in the experiment. One of these complexes is *cis*-diamminedichloroplatinum(II) or cisplatin which has been shown to be effective in treating testicular, ovarian, lung, head and neck, bladder and cervical cancers.

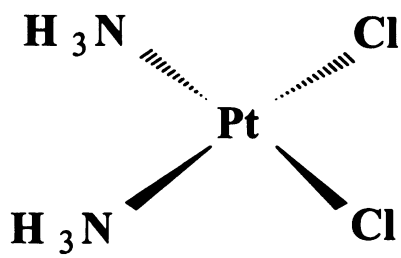

Figure 1. Schematic of the Cisplatin Molecule

A. Mechanism of Action for Cisplatin

After many decades of investigations, researchers have compiled a large database of information about how cisplatin is metabolized. The chloride ligands of cisplatin are stable with respect to substitution at high chloride concentrations such as those found in the extracellular matrix, but when the compound diffuses into the cell, the lower chloride concentration causes loss of chloride ligands and replacement with water.[2] The resulting mono and bis-aqua complexes are reactive with nucleophilic sites of cellular macromolecules. The effect of this inorganic compound on the synthesis of RNA, DNA, and proteins has been evaluated, and it was found that at high concentrations and long incubation periods, the synthesis of these three biomolecules is inhibited.[3] DNA synthesis is preferentially inhibited at all concentrations, thus DNA is thought to be the most likely target of cisplatin with respect to its chemotherapeutic properties.

In order to understand the suppression of DNA synthesis by cisplatin, it is important to consider the nature of this macromolecule. DNA is a polynucleotide chain composed of nucleotides that are phosphate esters of pentose with nitrogenous bases linked to them (Figure 2). The standard nomenclature for nucleic acids establishes numbering from 1 to 9 for the

base and numbers from 1' to 5' for the sugar moieties. The hydrogen atoms retain the same label of the carbon to which they are attached. In the case of where there is more than one hydrogen atom on the same carbon atom, ie, CX' (X=H), the second hydrogen atom is labeled as CX''. The base is attached at the 1' position of the sugar residue, which, in this case, is a deoxyribose since it has only one hydroxyl group located in the 3' position. The bases are derivatives of purines and pyrimidines, and are responsible for the specificity of the sequence of DNA. This sequence defines the structure and coding for further transcription of DNA into RNA and final translation into proteins. The purine bases are guanine (G) and adenine (A) while the pyrimidine bases are cytosine (C) and thymine (T). The polynucleotide chain presents an orientation from the 5' end to the 3' end which are the positions where the phosphate group binds to the deoxyribose.

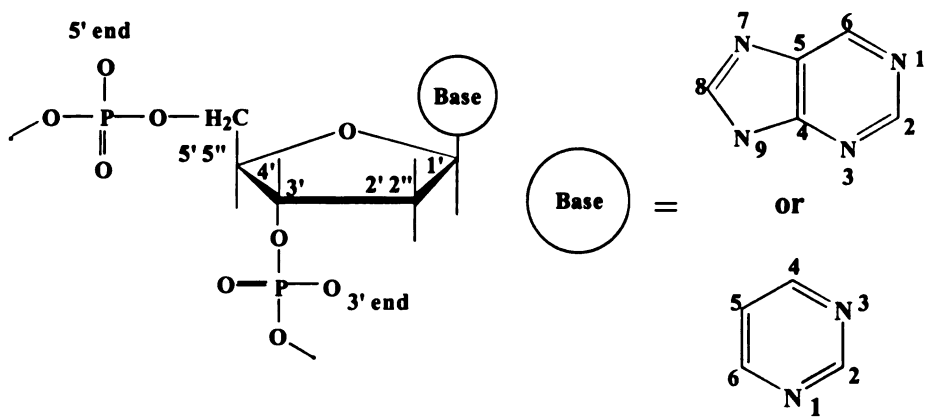

Figure 2. Nucleotide Structure Showing Labeling Scheme

The most common form of DNA consists of two strands wound about a common axis in an antiparallel and helical fashion forming a right handed 5' to 3' helix. The strands are held together by hydrogen bonds formed between the bases of each strand, thereby forming base pairs. The most stable base pairs are those formed between guanine (G) and cytosine (C) and between adenine (A) and thymine (T). These bases are called the Watson-Crick base pairs. The double stranded DNA is then formed with the phosphate backbone at the periphery (hydrophilic region) in contact with the solvent, keeping the bases in the core (hydrophobic region) of the helix. Because the base-pairs are not exactly in the center of the helical axis, the DNA helix possesses two grooves with different widths and depths; these are the major and minor grooves (Figure 3).

Double helical DNA can be classified into three types, namely, A, B, and Z-DNA, which exhibit fundamental differences in base stacking along the strand and in the conformation of the sugar-phosphate backbone. Among these three types, B-DNA is considered the native form because its X-ray pattern resembles that of DNA in intact sperm heads.[4]

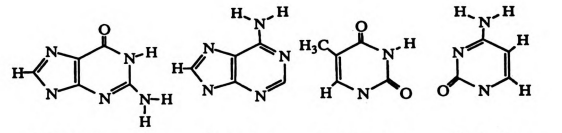

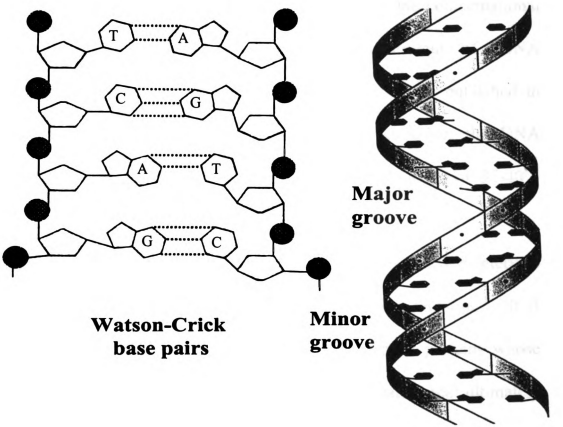

Figure 3. Schematics Depicting The Basic Structure of DNA

The biological action of cisplatin is linked to the formation of stable Pt-DNA adducts. Major products of Pt-DNA binding involve the (N7,N7)-didentate cisplatin cross-link between two intrastrand adjacent guanines (GpG) or adenine-guanine (ApG) (Figure 4a,b). Minor products are intrastrand cross-links between two guanine residues separated by one nucleotide residue and interstrand cross-links between two guanine residues (Figure 4c,d).[5] These cross-links have been implicated for the biological activity of cisplatin because they produce distortions in the conformational structure of DNA.[6] Distortions observed in an X-ray structure of a DNA oligonucleotide of twelve base pairs bound to cisplatin was published in 1996 by S. J. Lippard and co-workers. In this structure, the DNA oligonucleotide exhibits a bent conformation with an angle of 35-40°.[7] Unwinding of the duplex was also observed.

It is presumed that the distortions caused by cisplatin have deleterious effects on replication and transcription, thereby causing mutation.[8] It is hypothesized that these lesions are recognized by certain proteins whose binding prevents the lesions from being repaired, a situation that ultimately leads to cell death. Such recognition is specific and requires a "kinked" DNA conformation.[9]

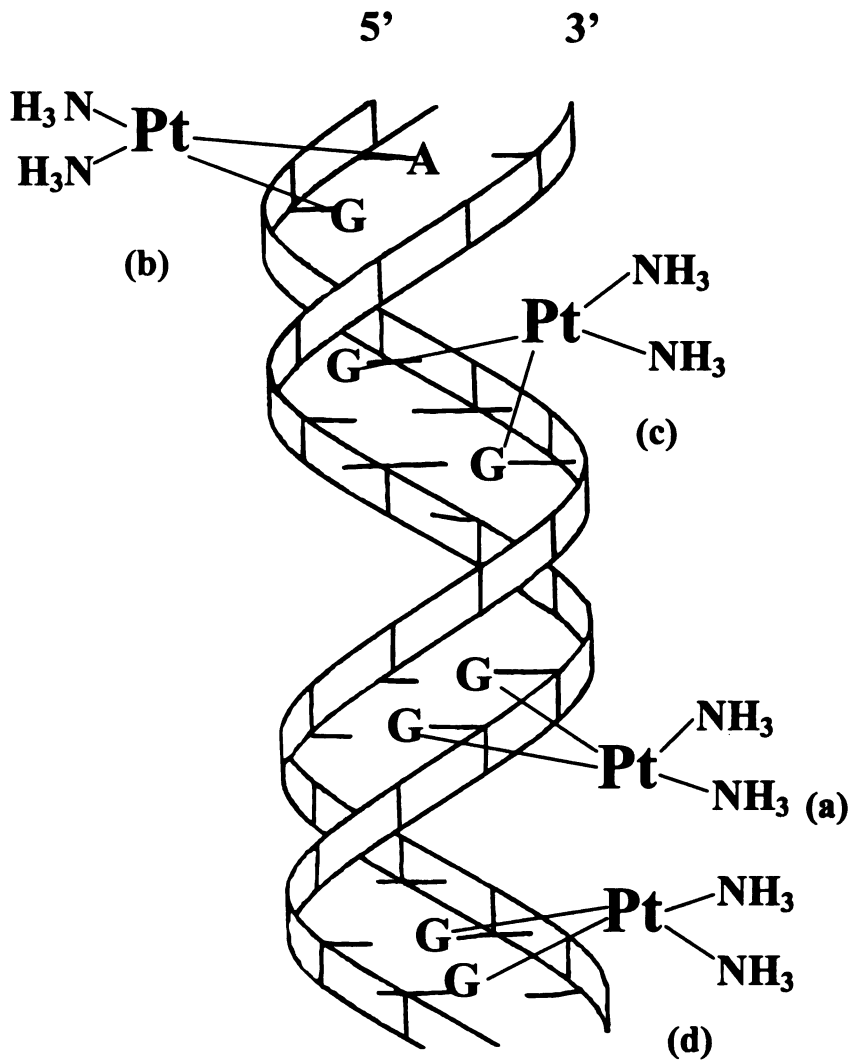

Figure 4. Cisplatin-DNA Inter- and Intrastrand Adducts

Some of the binding proteins have been identified as the high mobility group (HMG) domain proteins. Recently, it has been discovered that proteins responsible for mediating the biological processes of recombination, replication and transcription require the presence of DNA in an unwound and bent form and contain one or more HMG domains.[10]

HMG domains are α-helical structures that contain a high proportion of proline, aromatic and basic amino acids. Some of these HMG domain proteins, such as SRY and LEF-1, bind to specific DNA sequences via their hydrophobic residues. These domains behave as intercalators, causing unstacking of several base pairs, which leads to unwinding and bending of the DNA.[11] Similar structural distortions have been observed when cisplatin binds to a DNA duplex.[12] One of the latest reports on this subject, published in 1997, established the high binding affinity and specificity of the murine testis-specific high mobility group protein, tsHMG, to cisplatin-modified DNA.[13]

It has been shown that the *trans* isomer of cisplatin, namely *trans*-DDP, enters the cells and binds to DNA like cisplatin.[14] Experiments performed *in vitro* have shown that, initially, *trans*-DDP binds more rapidly than cisplatin, but, with time, the quantity of bound *trans*-DDP diminishes while the quantity of bound cisplatin continues to rise.[15] These results

suggest that preferential repair of *trans*-DDP adducts occurs over those of cisplatin, although the details of how *trans*-DDP is removed are still not well understood.

Interestingly, the HMG domain proteins studies also helped to explain the inactivity of the *trans* isomer. Now it is believed that the inactivity of *trans*-DDP is due to the specific binding of the HMG-domain proteins to cisplatin modified DNA. Although *trans*-DDP is capable of binding to only one strand in duplex DNA, it does so by forming a 1,3-intrastrand cross-link of guanine bases, *trans*-$[Pt(NH_3)_2\{d(G^*pNpG^*)\}]$[16], which leads to different structural alterations that are thought to be repaired more efficiently than the distortions produced by cisplatin.

More recently, experiments using *in vitro* transcription challenge competition assays demonstrated the capability of the promoter recognition factor involved in transcription, the TATA binding protein (TBP), to preferentially bind cisplatin damaged DNA in favor of normal binding sites. The consequence of this is the prevention (or at least reduction) of transcription.[17]

Despite its high anticancer activity, the use of cisplatin as a drug is mediated due to its highly toxic side effects. Patients who receive the drug as part of their therapeutic treatment are likely to suffer from renal toxicity,

hematologic deficiencies, hearing loss, nausea, neurotoxicity and cardiac abnormalities. In response to these problems, other platinum compounds with reduced toxicity such as carboplatin have been developed (Figure 5a). Results indicate, however, that carboplatin may be less effective against testicular cancer with respect to long term cures.[18] Presently, other compounds such as JM216 [19] (Figure 5b) and oxaliplatin[20] (Figure 5c) are in various stages of clinical testing. The former has been shown to exhibit lower toxicities than cisplatin and carboplatin. The latter appears to be promising for colon cancer treatment, but its use might be limited due to its high levels of neurotoxicity.

In spite of the promise of metal-based drugs, the battle against cancer continues, with studies being focused on both improved platinum compounds and on non-platinum metal compounds. New compounds may exhibit reduced toxicities, improved activities against cisplatin-resistant tumors or efficacy against cancers that are currently untreatable.

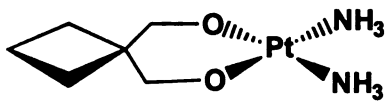

Carboplatin

(a)

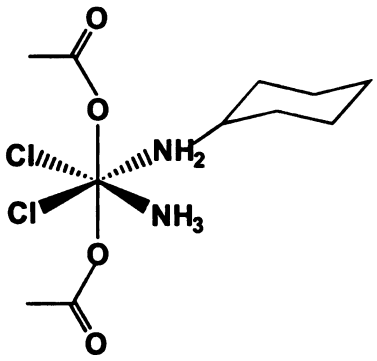

JM216

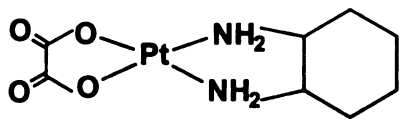

Oxaliplatin

(b) **(c)**

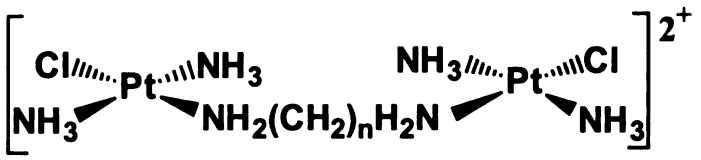

(d)

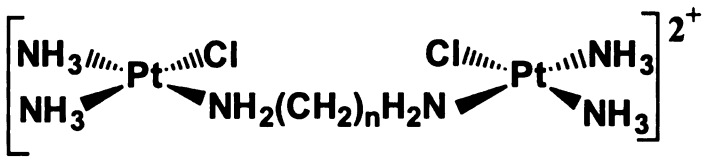

(e)

Figure 5. Biologically Relevant Platinum Compounds

B. Rhodium Carboxylates as Potential Anticancer Agents

In the search for new chemotherapeutic agents, studies were initiated with antitumor active compounds that may be capable of binding to bases in a manner similar to cisplatin. Dinuclear platinum and rhodium compounds fall into this category. Because of their wider "bite angle" for binding as compared to *cis*-DDP, there is a greater possibility that dinuclear compounds can form both intrastrand and interstrand cross-links.[21] Indeed, dinuclear platinum complexes structurally related to cisplatin such as the *cis*- and *trans*- isomers of $[\{PtCl(NH_3)_2\}_2H_2N(CH_2)_nNH_2]^{2+}$ (Figures 5d and 5e), have been tested for anticancer activity in mice and were shown to be effective against cisplatin resistant tumors. [22] The DNA binding mechanism of these compounds may be different from that of cisplatin, since it was found that in a d(GCGC) sequence, the preferred binding sites are interstrand over the favorite intrastrand -GG- cross-link of cisplatin.[23] Some of these dinuclear complexes promote a change in the conformation of DNA from the B type to Z-DNA.[24] Like cisplatin, they unwind DNA but they do not bend DNA in the same way. This may play a role in their efficacy towards cisplatin-resistant cells.

Among the group of non-platinum compounds that may exhibit binding modes similar to cisplatin are dimetal carboxylates. Instead of one square planar metal unit, they are composed of two approximate square planar units joined by a metal-metal bond (Figure 6). Over the years, it has been shown in our laboratories and others that the dimetal tetracarboxylate compounds react with incoming bases by displacing two cis RCO_2^- ligands, which means that they could react in a similar manner to cisplatin.

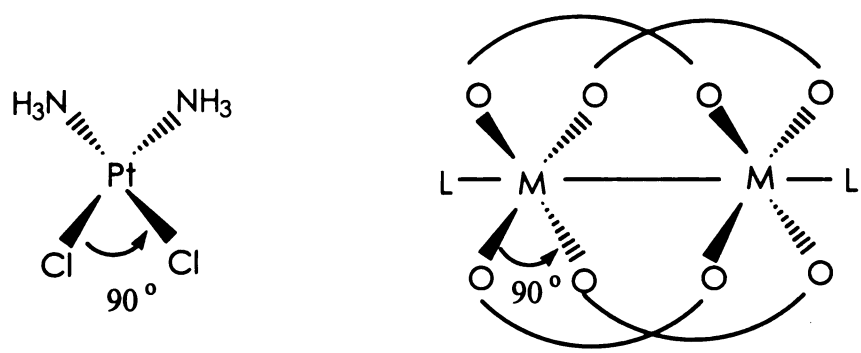

Figure 6. Comparison of Cisplatin and Dimetal Carboxylate Binding Sites

During the 1970's, studies of dirhodium carboxylate compounds revealed their potential as chemotherapeutic agents against certain tumors including Ehrlich ascites and L1210 tumor cells in mice. The strong inhibitory effect of the compounds on DNA but not on RNA synthesis *in vivo* was also demonstrated.[25] In these experiments, the anticancer activity of the compounds $Rh_2(O_2CCR)_4L_2$ (R = CH_3, C_3H_7, C_4H_9) was explored and it was found that the propionate and butyrate compounds exhibited higher

potencies than the acetate complex. The level of toxicity however, was invariant. Among the dinuclear rhodium carboxylates, the compound $Rh_2(DTolF)_2(O_2CCF_3)_2(H_2O)_2$ (DTolF = N,N'-di-p-tolylformamidinate) was also tested for antitumor activity with promising results against Yoshida sarcoma and T8 sarcoma of Guerin being obtained.[26] This compound exhibits reduced toxicity as compared to $Rh_2(O_2CCH_3)_4$ and cisplatin.

The early literature regarding the DNA binding studies of dirhodium carboxylates reported that these compounds were unreactive towards poly G DNA sequences but reactive towards poly A sequences and single-stranded DNA. This conclusion was based on the absence of color change during the reaction with guanine bases, while in the reactions with adenine bases a dramatic color change from blue-green to pink was observed. Reactions performed with 9-ethylguanine in our laboratories revealed that gaunine does indeed bind and in an unprecedented manner wherein two guanine bases are bound in a bridging mode. X-ray structures were determined and the compounds were found to contain *cis*- guanines with the N7 and O6 atoms coordinated in a "head-to-head" bridging mode (Figure 7a) or a "head-to-tail" bridging mode (Figure 7b).[27] The reactions were performed with 9-ethyladenine as well and it was found that N7,N6 bridges formed. These results support the conclusion that dirhodium tetraacetate has

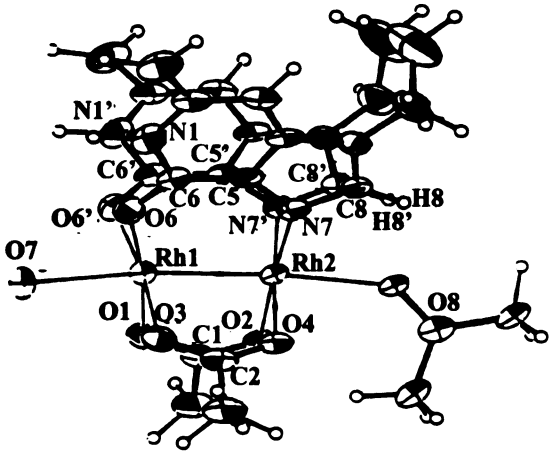

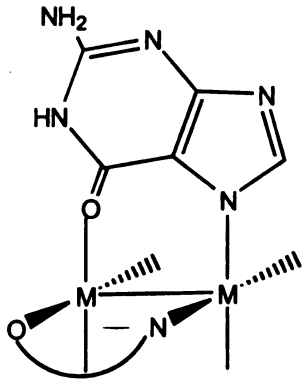

Head-to-Head

(a) $[Rh_2(O_2CCH_3)_2(9\text{-EtGH})_2(Me_2CO)(H_2O)]^{2+}$

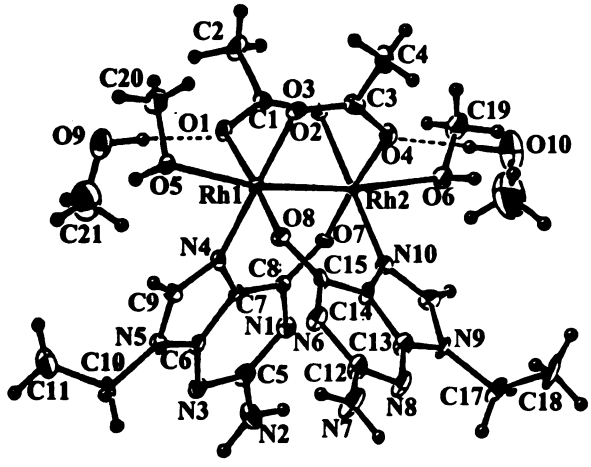

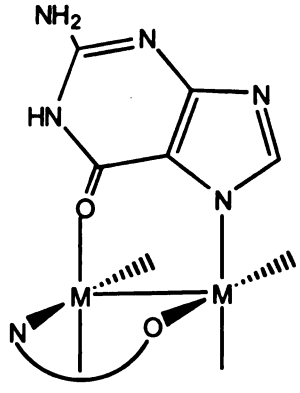

Head-to-Tail

(b) $Rh_2(O_2CCH_3)_2(9\text{-EtG})_2(MeOH)_2.2MeOH$

Figure 7. X-Ray Structures of Dirhodium Compounds with Guanine Bases

equatorial sites available for binding as well as axial sites.

C. NMR Analysis of Cisplatin-DNA Adducts

The aforementioned studies of dimetal compounds, which included single cystal X-ray structures of model purine reaction products, were the starting point for our studies of the DNA binding of dimetal carboxylate compounds. We began our current investigation from the perspective of what is known about cisplatin in order to make comparisons and contrasts to the behavior of dirhodium carboxylates under the same conditions.

Determination of the structural distortions of cisplatin-DNA adducts at the molecular level is important for the eventual understanding of cisplatin's activity. In addition to X-ray crystallography, NMR spectroscopy is an extremely valuable tool for probing DNA-adducts of cisplatin. The full mechanism of action of cisplatin as an anticancer agent may eventually be understood on the basis of both solution and solid-state structures of DNA/cisplatin/protein interacions.

Initial analyses of the distortions created by platinum complexes bound to DNA were conducted with di- and trinucleotides. The small size of these adducts renders them excellent candidates for study by NMR

spectroscopy, molecular mechanics and X-ray crystallography.[28] Distortions upon platination of DNA duplexes of ten, eleven and twelve base pairs were also investigated by 1D and 2D NMR spectroscopy.[29] In 1995, a more detailed 2D NMR analysis of an intrastrand *cis*-DDP-GG cross-link structure of an octameric DNA duplex was performed.[30] The DNA sequence selected for these spectroscopic studies was d(CCTGGTCC) d(GGACCAGG), represented in Figure 8.

```
     1  2  3  4  5  6  7  8
5'   C  C  T  G* G* T  C  C  3'
3'   G  G  A  C  C  A  G  G  5'
    16 15 14 13 12 11 10  9
```

G*G* = Platinated site

Figure 8. DNA Octamer Sequence Studied by ^{1}H NMR Spectroscopy

Some of the results of this work are the following:

(1) The conversion of the sugar conformation of the 5' platinated guanosine from C2' endo to C3' endo was confirmed (Figure 9), although the remainder of the sugar residues of the double helix were in the original B type DNA conformation (C2' endo).

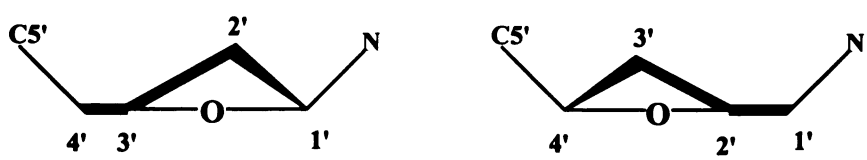

C2' endo; S type **C3' endo; N type**

Figure 9. Sugar Conformations

(2) The connectivities of both strands were generally uninterrupted with some variations in the intensity of the NOE cross-peaks from protons near the lesion site (Pt-G_4pG_5).

(3) The chemical shifts of G_4*H8 and G_5*H8 resonances were downfield in comparison with the other G resonances, indicating that both bases are platinated at their respective N7 positions.

(4) The G4 imino proton was not observed, presumably due to its rapid exchange with water.

The NOE restrained, refined structure of the modified duplex showed that the helix is kinked approximately 58° and unwound by –21°.

It should be noted that the structural features of this DNA sequence were obtained by using ^{1}H NMR spectroscopic data only, underscoring the importance of this analytical technique for these types of structural studies.

Chapter 2

1. APPLICATION OF NMR SPECTROSCOPY TO STRUCTURAL ELUCIDATION OF METAL-DNA ADDUCTS

The application of NMR spectroscopy to the study of biological macromolecules involves the analysis of NMR spectra in two or more dimensions. In these experiments, it is possible to observe through-bond couplings for nuclei separated by two, three or sometimes four bonds. Also, one can observe through-space connections between resonances of nuclei that are close to each other in space (≤5 Å), and exchange processes between resonances of the same nucleus in two different chemical environments. The structural information is principally obtained from measurements of the Nuclear Overhauser Effect (NOE), which provides constraints on internuclear distances, especially for small oligonucleotides. In addition to the determination of complete three-dimensional structures for macromolecules in solution, NMR provides valuable information on local structure, conformational dynamics and structural aspects of interactions with small molecules.

The principles of NMR spectroscopy are based on the behavior of the nuclear spins when they are placed in a static magnetic field (B_o). Each nucleus precesses around the field axis and by adding up all the z components of the nuclear magnetic moments, a macroscopic magnetization vector (M_o) along the field direction is obtained (Figure 10). In an NMR experiment, transitions are induced between the energy levels by irradiating the nuclei with a external magnetic field (B_1) originated from an electromagnetic wave of the suitable radiofrequency.

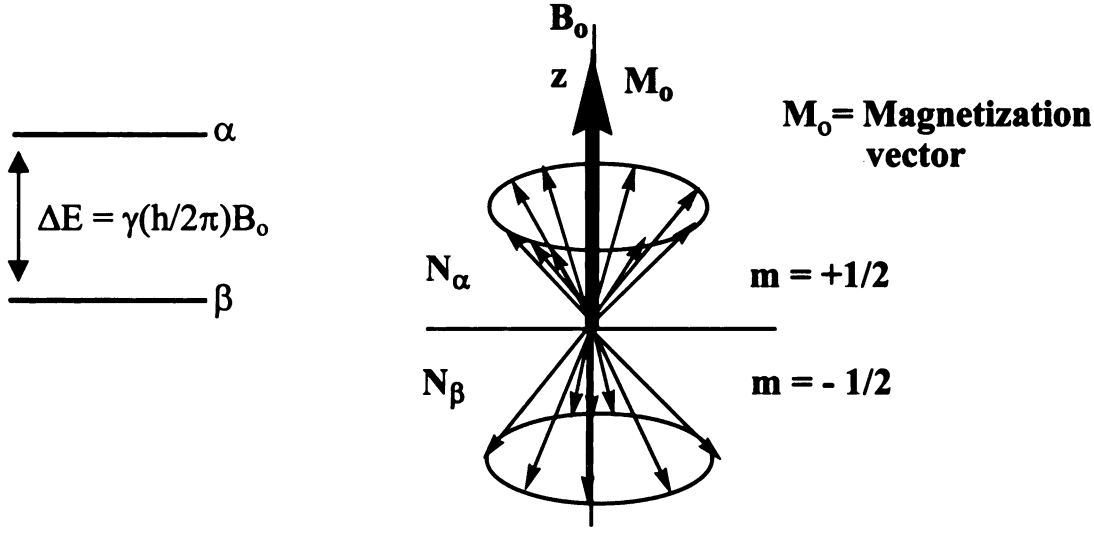

Figure 10. NMR Principle : Magnetization Vector

In the pulse experiment, a radio frequency pulse of duration τ_p (Figure 11a) is obtained by applying the magnetic field (B_1) along a specific

direction. This can be observed in Figure 11b where the x and y axes are rotating at the same frequency of B_1. The magnetization vector M_o is tipped away from the z axis by an angle that is dependent on the duration of the pulse and the strength of the magnetic field applied. The resultant vector (M_y) is called the transverse magnetization vector. This vector is important because it represents the NMR signal since the detector contains the receiver coil aligned along the y direction.

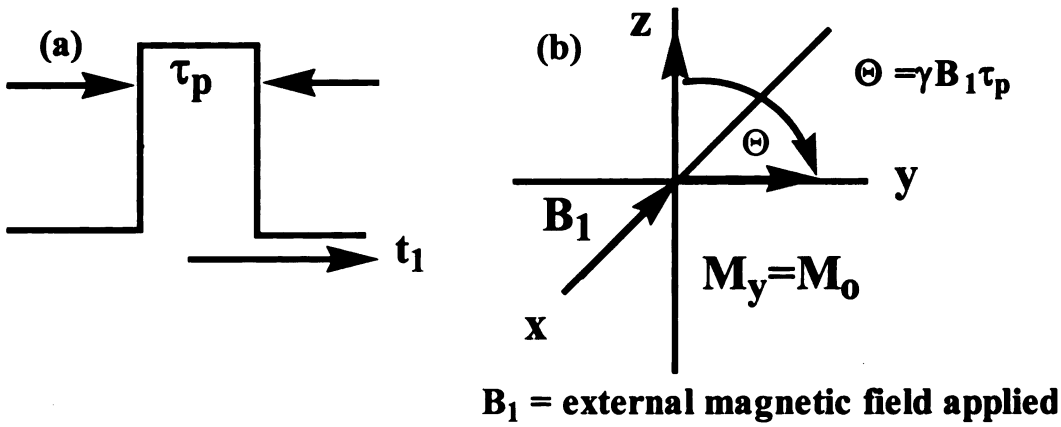

Figure 11. Pulse Experiment

A. Solvent Suppression Techniques

For a thorough understanding of NMR processes in nucleic acids, it is important to differentiate between two types of protons in these biomolecules. This classification stems from the ability or inability of these protons to exchange with protons of the solvent. The exchangeable types

include the protons A (NH_2)6, G (NH_2)2 and G(NH)1, T(NH)3, and C(NH_2)4 with the remainder of the protons present in the molecule being non-exchangeable. In order to detect the exchangeable protons, the sample must be dissolved in a protonated, rather than deuterated, solvent. Unfortunately, this presents the problem of dealing with a very high concentration of water compared with the sample concentration, diminishing tremendously the dynamic range of the instrument and the intensity of the resonances of interest. For this type of analysis either selective excitation or solvent suppression NMR techniques must be performed in order to overcome this problem.

Among the selective excitation methods, the binomial method is commonly used. The method uses a selective excitation pulse sequence which produces a non-excited region around the solvent chemical shift while causing significant excitation in the region of interest. The magnetization process can be explained by looking at one of the simplest pulse sequences, the 1-1 sequence (Figure 12). In this sequence, the excitation pulses are placed at one end of the spectrum, separated by N Hz, where N represents the distance from the solvent resonance frequency to the region to be excited. All the pulses have the same phase and are separated by a delay time ($2N^{-1}$) in seconds.

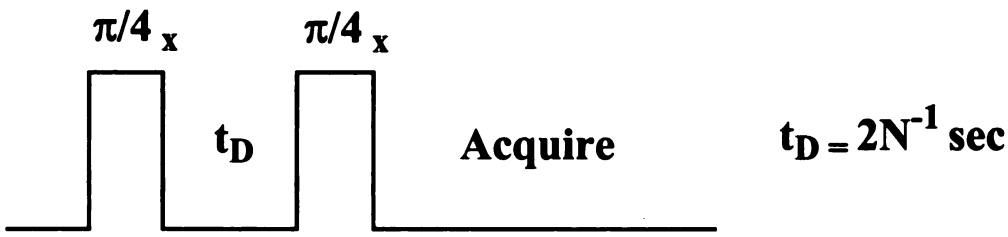

Figure 12. Binomial 1-1 Pulse Sequence

By observing the magnetization process for the solvent signal using the vector diagram shown in Figure 13, one can observe that after the two pulses, the magnetization vector returns to its initial position along the z axis, therefore yielding no net excitation of this signal.

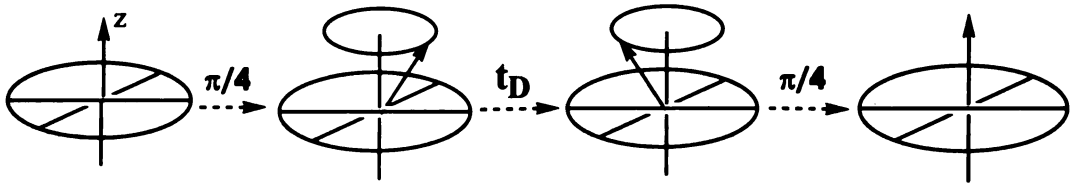

Figure 13. Solvent Magnetization Vector for 1-1 Sequence

The magnetization vectors that do not precess at frequencies multiples of N Hz however, will not be aligned in the yz plane before the second pulse; instead, they will experience a net excitation. According to their precession frequency, they will resonate before or after the solvent signal, resulting in a 180° dephased spectrum. The intensity of the signal as a

function of frequency offset with respect to the solvent resonance is shown in Figure 14. From this picture, it can be noted that it is important to set the frequency offset appropriately for maximum excitation of the region of interest. Other pulse sequences are called 1-2-1 and 1-3-3-1 which provide a wider zero excitation around the solvent signal.

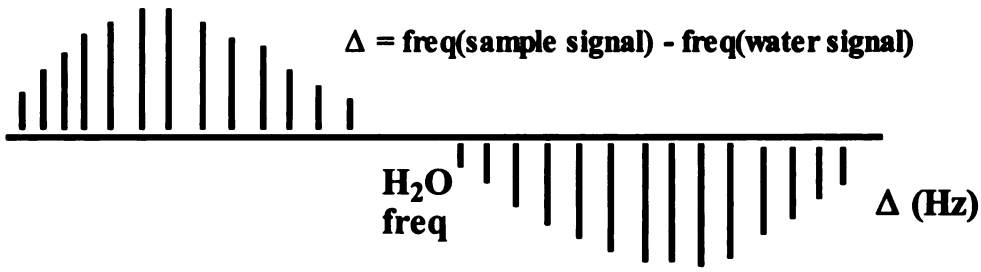

Figure 14. Signal Intensity as Function of Frequency Offset

Water suppression techniques are also very useful and effective for NMR analysis of biomolecules. The development of actively shielded probes that can produce high-power field gradient pulses has resulted in new experiments that make use of these field gradients instead of phase cycling for selection of coherences. A field gradient pulse can be defined as a period during which the magnetic field B_o is made intentionally inhomogeneous. In this field, the nuclear spins along the NMR sample experience different

magnetic fields, and thus transverse magnetization and other coherences dephase across the sample. (Figure 15). The coherence can be refocused by another appropriately applied gradient to generate gradient echoes.

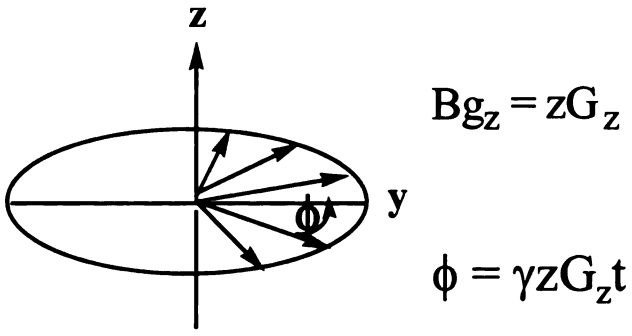

Figure 15. Gradient Pulse Effect on Magnetization

An example of this technique is the Water Suppression by Gradient Tailored Excitation (WATERGATE),[31] whose pulse sequence is shown schematically in Figure 16.

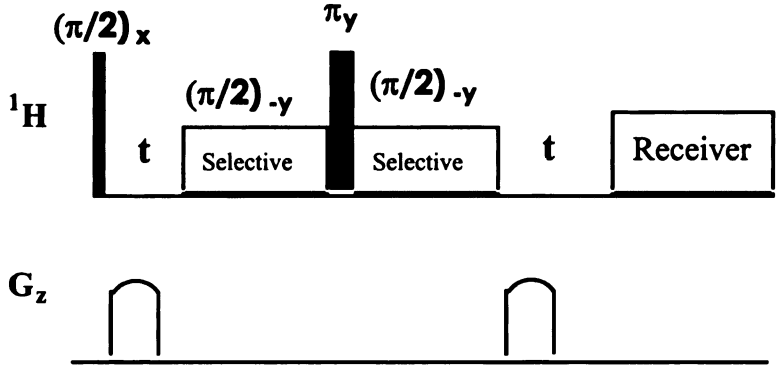

Figure 16. WATERGATE Pulse Sequence

The gradient pulses (G_z), shaped as a smooth function of time, are used to remove the unwanted coherences. Following the initial non-selective pulses, a field gradient dephases the solute and solvent magnetizations. The former is not affected by the selective pulses. The non selective π pulse inverts the coherence order of the solute magnetization and, in this way, the second gradient pulse rephases the solute magnetization to form a gradient echo. On the other hand, the combination of selective and non selective pulses leaves the coherence order of the solvent magnetization unchanged. The consequence of this is complete dephasing of this signal after the second pulse gradient is applied and no echo is formed. This technique provides highly efficient suppression of the water signal.

B. Two-Dimensional NMR

Two-dimensional NMR analysis of biomolecules, provides a variety of techniques for obtaining information on a molecule in three dimensions. One of the most important techniques is Nuclear Overhauser Effect Spectroscopy, or NOESY which correlates protons that are separated by distances as great as 5 Å. This technique is based on the Nuclear Overhauser Effect, or NOE, which is the change in intensity of a resonance due to the perturbation of transitions of another resonance.

$$\eta_{I=}(I-I_o)/I_o,$$

where I_o represents the equilibrium intensity. This change is a consequence of the modulation of the dipole-dipole coupling between different nuclear spins produced by the motion of the molecule in solution. In a spin network contained in a macromolecule, spin diffusion by two or several subsequent relaxation steps among nuclear spins in proximity, can also take place and influence the observed NOE intensities.

For two I= ½ uncoupled spin nuclei with different chemical shifts, the energy level system is represented in Figure 17. The αβ and βα levels are not at the same energy because the proton nuclei do not have the same chemical shift which renders them inequivalent.

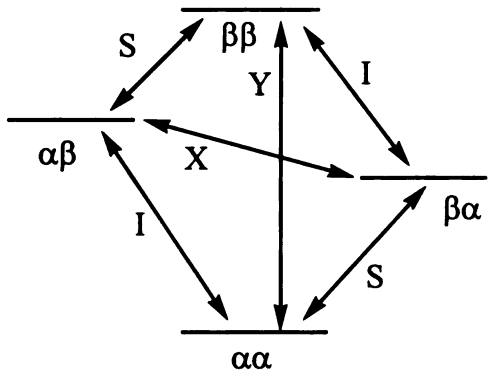

S,I = Observable transitions

X,Y = Non observable transitions

Figure 17. Spin State Observable and Non Observable Transitions

There are two observable transitions, indicated by I and S, as well as two non-observable transitions, represented by X and Y, which may contribute to the relaxation processes. The relaxation through observable transitions is a first order relaxation process (W_1) while the relaxation due to non-observable transitions is denoted as W_o for X, which is the zero-order transition, and W_2 for Y, which is the second-order transition. Therefore the relaxation process is a result of the combination of W_o, W_1, and W_2, because

now a saturation of spin S will affect the intensity for spin I. These zero and second order transitions are responsible for the detection of an NOE.

The local field that one spin experiences due to the presence of another spin will depend on the orientation of the molecule. In solution, rapid molecular motion averages the dipolar interaction, generating fluctuating fields which stimulate longitudinal relaxation (T_1). Furthermore, the strength of these interactions depends on the internuclear distance. Therefore we can say that the intensity of an NOE will depend indirectly on the distance r between pre-irradiated and observed spins, and directly with respect to the correlation time, τ_c, which is the average time for the molecule to rotate through one radian. The NOE is a population effect; therefore, it will influence the intensities of the resonances since they are proportional to the difference in population of the energy levels between which the nuclear transition occurs.

$$\text{NOE} \quad \alpha \quad (1/r^6).\tau_c$$

The pulse sequence for NOESY is shown in Figure 18. A variable delay time t_1 is inserted after the first pulse, thereby allowing the different nuclear spins to precess according to their frequencies in the XY plane. The second pulse brings the magnetization vector back to the z axis.

Magnetization transfer due to dipolar coupling takes place during the mixing time, τ_m, before observable transverse magnetization is created by the final 90° pulse. Finally, the signal is detected and recorded during the acquisition time t_2. Fourier transform with respect to t_2, corresponds to the first dimension of the spectrum while Fourier transform with respect to the delay time, t_1, corresponds to the second dimension of the spectrum. The cross-peaks will consist of responses corresponding to the size of the NOE that was built up during the mixing time. By looking at the intensity variation as a function of this time, distance information can be extracted from the spectrum.

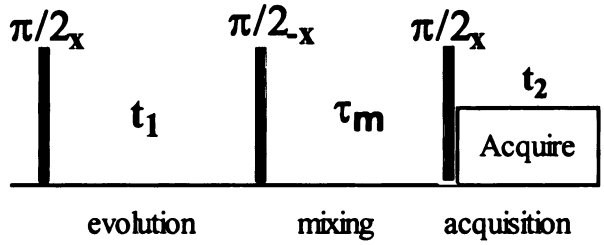

Figure 18. NOESY Pulse Sequence

One important preliminary experiment for any DNA sample prior to a NOESY experiment is the measurement of T_1, or longitudinal relaxation time. The value of T_1 is defined as the time required for the magnetization

vector representing a certain spin to return to its equilibrium state along the z axis. This measurement can be obtained by performing an Inversion Recovery experiment. This experiment records a series of spectra using the following sequence:

$$\mathbf{180^{\circ}_{x} - t - 90^{\circ}_{x} - Aquisition}$$

The value of t changes for each spectrum. The behavior of the magnetization vector is illustrated in Figure 19.

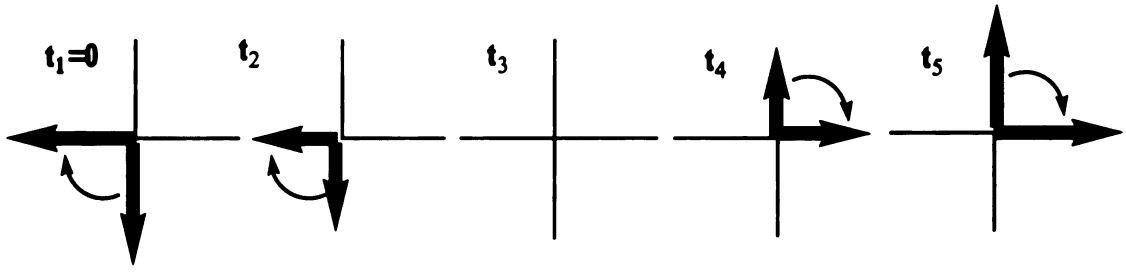

Figure 19. T_1 Measurement : Inversion Recovery Experiment

As t varies, the amplitudes of each signal changes in different ways. The next 90° pulse will give an observable transverse magnetization. A return to equilibrium will take place through relaxation associated with the transfer of energy from the spin system to the surroundings (spin-lattice relaxation). This relaxation will occur at a rate determined by T_1 based on the following equation,

$$dM_z / dt = (-M_z - M_0) / T_1$$

where $M_z = -M_0$ at t=0; resolving this equation:

$$\ln(M_0-M_z) = \ln 2M_0 - t/T_1$$

Therefore, by plotting $\ln(M_0-M_z)$ against t, the value of T_1 can be calculated from the slope of the straight line obtained.

Fully deoxygenated samples of duplex DNA exhibit T_1 values for the H2 protons of adenosine in excess of 3 sec. The long T_1 values for these isolated protons require long recycle delays to be implemented between transients during acquisition of NOESY data to allow for full recovery of their signals. Another important factor for NOESY is obtaining data of adequate signal-to-noise ratio and sufficient digital resolution. Acquisition of NOESY data with good digital resolution in t_2 is possible with the help of computers. However, the acquisition of NOESY data with sufficient digital resolution in t_1 requires making a compromise between high signal-to-noise in each increment when the value of t_1 is varied, or acquiring more increments with reduced signal-to-noise. By using linear prediction (LP) as part of the data processing, the need for this compromise can be eliminated. In many cases insufficient t_1 points are acquired during NOESY to permit an interferogram signal to decay to zero. Forward LP can be used in these cases to extend the data.

Linear prediction is based on singular value decomposition (LPSVD). This is a digital processing technique that assumes each interferogram in the F_1 dimension or free induction decay (FID) in the F_2 dimension is a series of exponentially decaying cosine or sine functions. Therefore, linear prediction allows one to extend these mathematical functions to longer acquisition (t_2) or evolution (t_1) times. The frequencies, amplitudes and phases for the signals can be calculated from any portion of the data. Furthermore, with LP, the amplitudes of the signals of the FID are determined only from the experimental data, having unaltered intensities for the NOESY experiment extended with LP. It also provides resolution enhancement, allowing for the evaluation of volumes for cross- peaks that are closely spaced, which would be poorly resolved in the NOESY spectra without LP. Therefore, the utility for using linear prediction as a data processing tool has become very important in terms of obtaining better spectra and reducing acquisition time.

Among NMR techniques involving scalar coupling spins, Total Correlation Spectroscopy or TOCSY is a very useful technique for elucidating direct coupling in biomolecules. TOCSY uses a pulse sequence in which an isotropic mixing time is included. In this sequence, the chemical shift terms are eliminated over a significant frequency range while the spin locking radiofrequency field is applied. Magnetization transfer

under the influence of such a sequence, results in a continuous mixing process with the magnetization moving periodically among all the spins in the scalar coupled network. In this way, all the spins that belong to this network can be connected. The isotropic mixing time can be varied in order to obtain either efficient transfer of magnetization through a single three-bond scalar coupling only or maximum transfer of magnetization between resonances at extreme ends of a spin system. Both of these aims cannot be accomplished by using a single mixing time, therefore experiments using different τ_m values are recommended. The range of variation of τ_m is from 50 to 100 ms.

The basic pulse sequence for a TOCSY experiment is presented in Figure 20. After frequency labeling during t_1, magnetization is returned to the z axis for the isotropic mixing process to take place. After that the magnetization is rotated to the transverse plane for detection.

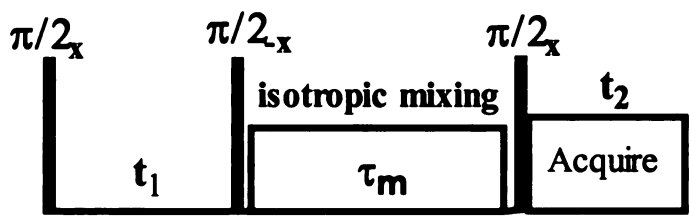

Figure 20. TOCSY Pulse Sequence

The observation of the cross-peak between two spins in the TOCSY experiment does not necessarily indicate that the spins are directly coupled; the magnetization is transferred between them by a series of steps through two- or three-bond scalar couplings between mutually coupled spins.

In most cases, the assignments of the majority of the proton chemical shifts of a complex DNA molecule are possible by using a combination of different 2D NMR experiments. Usually NOESY and TOCSY are the most important and useful ones. However, sometimes these methods are not sufficient to allow for information to be obtained from overlapping areas of the spectrum, especially those close to the diagonal. Furthermore, with TOCSY, magnetization transfer through the H3' protons can be poor due to the unfavorably low values of the H3'-H4' coupling constants found in B-form DNA. Furthermore, the use of the isotropic mixing pulse for a long period of time can produce heating of the sample. These problems can be eliminated by using an adjusted phase-sensitive 2Q COSY experiment.[32] Here, direct correlations are present as pairs of cross-peaks at mirror-image locations about the double quantum diagonal, where the chemical shift in F_1 is the sum of the single-quantum chemical shift in F_2. One of the advantages of the 2Q COSY experiment is the absence of diagonal peaks in the

spectrum. It also provides direct and relayed correlations if an adequate pulse-phase is applied. Furthermore, these correlations are easy to separate since the direct ones are symmetrical about the double-quantum diagonal while the relayed correlations are not; therefore, the separation can be made by symmetrization about the double-quantum diagonal.

The pulse sequence of 2Q COSY is presented in Figure 21. The first three pulses are dephased by 45° with respect to each other. Following the initial 90° pulse, an antiphase coherence is developed during a fixed spin-echo sequence. This is in contrast to COSY experiments in which antiphase coherence is developed during t_1. The 180° pulse re-focuses the chemical shift evolution. Multiple-quantum coherence is generated by the second 90° pulse and the precession of the desired 2Q state is monitored during the t_1 period. The final 90° pulse creates observable single-quantum magnetization which is recorded during t_2.

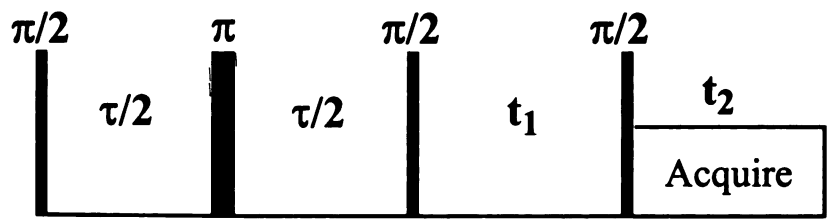

Figure 21. 2Q COSY Pulse Sequence

Chapter 3

1. EXPERIMENTAL SECTION

The work in this chapter was developed along similar lines to previous studies carried out with cisplatin. Samples of dirhodium carboxylate compounds and DNA oligonucleotides were reacted and the products analyzed by ^{1}H NMR spectroscopy. In order to establish a comparison between the native and dirhodium-bound DNA, a detailed analysis of the native DNA oligonucleotide sequence was first undertaken.

The DNA sequence selected for these studies is d(5'-CCTCTGGTCTCC-3') ·d(3'-GGAGACCAGAGG-5'). There are several characteristics of this sequence that render it desirable for this study. The presence of two consecutive guanine bases in the middle of one strand allows for only one binding site for the dirhodium carboxylate molecules on this oligonucleotide. Furthermore, the 2D ^{1}H NMR analysis of a very similar sequence, although with fewer base-pairs, has been performed with the cisplatin work. A summary of these findings was presented earlier. This

NMR analysis will allow us to make an adequate comparison of the previous studies with our work. Additionally, since the platinated adduct of this 12-mer sequence was structurally characterized, there is good potential for obtaining a crystal structure of the dirhodium-DNA adduct as well.

A. DNA Purification

In order for a sample to be analyzed by NMR spectroscopy, it must be very pure. Any contamination from residual oligomers of shorter lengths leads to complications in the NMR spectra from the presence of more than one DNA population. Contamination due to the presence of metal di-cations is also a concern since they bind strongly to DNA. Procedures used in the elimination of these two contaminants will enrich the sample with salts which have to be removed as well.

Obtaining purified DNA oligomers is limited by the available technology for the synthetic process. Synthetic oligonucleotides of x-bases are contaminated by varying proportions of "failures", *i.e.*, oligonucleotides of lengths x-1, x-2, ..., x-(x-1). Separation of the 12-mer oligonucleotide from the mixture was performed by ionic exchange chromatography using a Perkin Elmer LC 235 HPLC instrument. A Source Q15 of 15 microns bead

size (Pharmacia) was used as the stationary phase. The eluants used for the mobile phase were a combination of low and high salt concentration solutions labeled as A and B:

Eluant A : 0.1 M NaOAc, 20% CH_3CN

Eluant B : 0.1 M NaOAc, 20% CH_3CN , 1 M KCl

For the separation to be effective, the process was performed by using the following gradient :

Time(min)	%A	%B	Flow Rate (mL/min)
0	100	0	4
5	70	30	4
65	65	35	4
70	0	100	4
75	0	100	4
80	100	0	4

In this gradient, the salt concentration is increased rapidly during the first five minutes in order to allow for the shorter-length, less highly charged, oligonucleotides to elute first. The salt gradient then becomes more shallow which allows for separation of the oligomers of higher charge, (especially the 11-mer and 10-mer oligonucleotides) from the one of interest, namely the purified 12-mer. This process was performed for both strands.

The HPLC chromatograms are presented in Figure 22. Each of the residues was observed by using UV detection with a wavelength of 260 nm. The retention time for each 12-mer strand was typically 30 minutes.

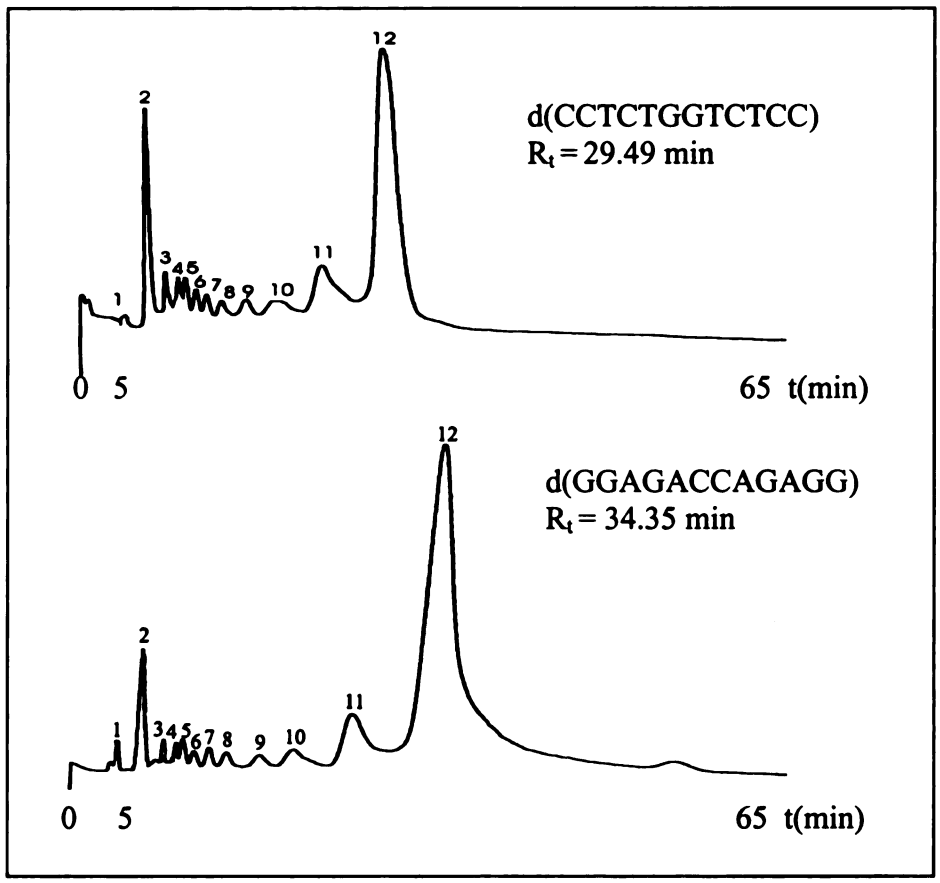

Figure 22 - HPLC Chromatogram of DNA Strands

After purification of each 12-mer strand, the sample was concentrated to reduce the volume of the fractions. In order to eliminate metal ions, a

chelating ion exchange resin called CHELEX (BIORAD) was added in amounts of 1 g per each 30 mL of sample. CHELEX consists of a sodium salt of a styrene divinylbenzene copolymer that contains paired iminodiacetate ions which act as chelating groups in binding polyvalent ions with a selectivity for divalent over monovalent ions of 5000 to 1. The sample was incubated with this resin overnight with constant stirring during which time the divalent ions were exchanged for Na^+ ions. The DNA was separated from CHELEX by passing the sample through a small column. The resin residue was rinsed with three 1 mL aliquots of a 1 M NaCl solution to extract residual DNA. The sample was then passed through a Sephadex G-25 fine pore size exclusion column (Pharmacia) in aliquots of 17 to 22 mL for desalting. The size of the columns was 75 x 2.5 cm in order to provide efficient separation. The desalted sample was evaporated to dryness, giving the pure DNA 12-mer strand as a transparent film. This process was performed for each strand. The purification yield for each strand was determined by measuring the absorbance at 260 nm using the experimentally determined extintion coefficient, ε, of 10,133 M^{-1} cm^{-1} for d(CCTCTGGTCTCC) (GG strand) and 13,467 M^{-1} cm^{-1} for d(GGAGACCAGAGG) (CC strand). The yield was between 30-50% for

both strands. Later, this yield was improved by changing the eluant composition to:

Eluant A : 10 mM NaOH , 200 mM NaCl

Eluant B : 10 mM NaOH , 1 M NaCl

The gradient used with these eluant times was similar to the one employed earlier, although the composition of A ranged from 64% to 59% during the 60 minute elution period. This change in eluant composition and elution profile increased the purified oligomer yield to 60%.

Once purified, both strands were mixed in an equimolar ratio. The mixture was allowed to stabilize for about 30 minutes and then heated to 60 °C and slowly cooled to room temperature to improve annealing. In order to eliminate any excess single strand, the sample was spun on a centriprep 3 centrifugal concentrator (Amicon), having a membrane with a molecular weight cutoff of 3 kDa which is slightly smaller than the double-stranded 12-mer. Excess single strand passes through the membrane, with the purified 12-mer oligonucleotide being retained in the upper sample chamber.

B. NMR Sample Preparation

The NMR sample was first prepared in H_2O to allow for detection of the exchangeable protons. An appropriate stock NMR buffer was added to the sample to obtain a final concentration of 10 mM Na_2HPO_4/NaH_2PO_4, 50 mM NaCl and 0.1 mM $NaC_2H_6AsO_2$ (sodium cacodylate). The pH of the sample is 7 in 0.25 mL final volume.

The NMR tube used for all of the experiments was a Shigemi tube that allows for the analysis of a small volume of sample, therefore minimizing problems with the signal-to-noise ratio for low concentration samples. In a Shigemi tube, the sample is enclosed between two glass plugs that have been treated in such a way that their permitivity is equal to that of the solvent used for all the experiments which in our case is water. In this way, the sample volume can be reduced in order to equalize the length of the radiofrequency coil of the instrument. When the sample is introduced into the tube, an air bubble is produced at the sample/upper glass plug interface. This bubble can be eliminated by placing the sample in a centrifuge and spinning it for 5-10 minutes at 1500 rpm.

C. ^{1}H NMR Analysis of DNA Dodecanucleotide

The NMR spectra were collected on Varian VXR 500 and UNITY INOVA 600, 500 and 600 MHz spectrometers. A WATERGATE experiment in 90% H_2O/10% D_2O was performed at 25 °C on the INOVA 600 which is programmed with the pulse field gradients needed for this experiment. This spectrum allows for the non-exchangeable and exchangeable protons to be observed. Only 10% of the deuterated solvent is necessary for locking the radiofrequency signal. The spectrum obtained is shown in Figure 23. It is important to point out that the water resonance at 4.769 ppm has been completely suppressed without distortion of the baseline or elimination of the sample resonances demonstrating the effectiveness of the WATERGATE pulse sequence for solvent suppression.

Using this first 1D spectrum, the basic proton regions in nucleic acids were assigned. The protons chemical shifts were identified by using the ranges presented in Table 1.[33]

Table 1. Chemical Shifts for Exchangeable and Non-Exchangeable Protons in DNA

Label	δ(ppm)
2' H , 2" H	1.8 – 3.0
4' H , 5' H, 5" H	3.7 – 4.5
3' H	4.4 – 5.2
1' H	5.3 – 6.3
CH_3 of T	1.2 – 1.6
5 H of C	5.3 – 6.0
6 H of C and T	7.1 – 7.6
8 H of G and A , 2 H of A	7.3 – 8.4
NH_2 of A, C, and G	6.6 – 9.0
NH of G and T	10 - 15

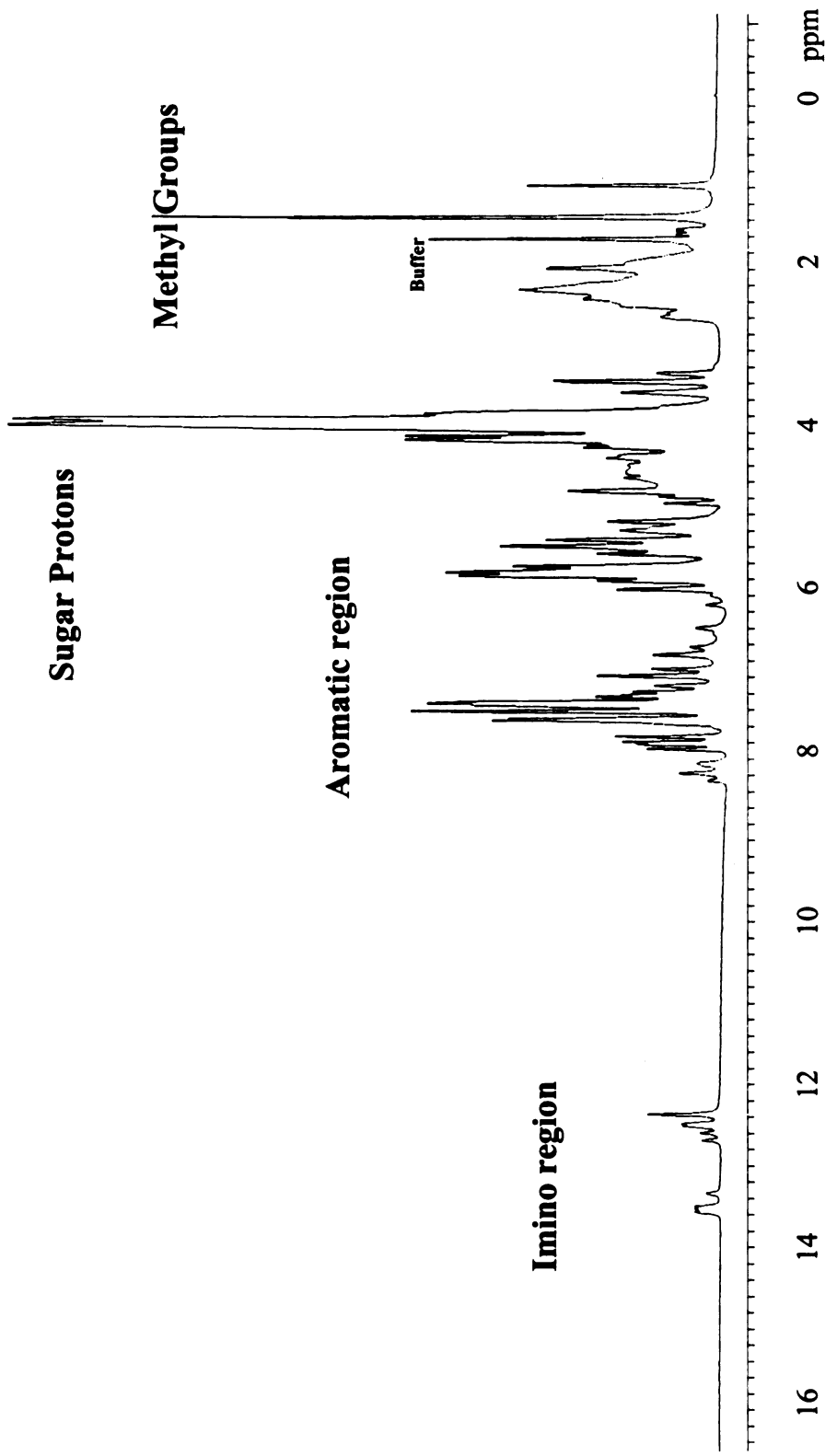

Figure 23 - DNA 12-mer ^{1}H NMR Spectrum in 90% H_2O at 25 °C

A series of 1D experiments at different temperatures were performed using the binomial 1331 sequence; these spectra are presented in Figure 24. The differences in chemical shifts and intensities are remarkably obvious as the temperature increases by 5 °C for each spectrum.

The A-T imino proton resonances of the duplex DNA are located further downfield with respect to the G-C imino proton resonances. The observation of the hydrogen-bonded imino protons in a Watson-Crick base-paired system represents direct evidence for the formation of the double-helical structure of the DNA dodecanucleotide. By examining these spectra, it can be noticed that, at room temperature, only ten out of twelve resonances are observed due to fraying of the ends of the duplex which allows for a rapid exchange with water. At lower temperatures, the line-width of the resonances increases due to a decrease of the rate of tumbling of the molecule; the rate of fraying also diminishes. As a consequence, it is possible to observe the imino protons at both ends of the duplex. For this sequence the ends consist of G-C base pairs for which resonances can be observed at 12.6 and 12.8 ppm at 5 °C. As the temperature is increased, the line-widths of some of the resonances become sharper in such a way that at 20 °C the four A-T imino base pairs are clearly observed while some of the G-C imino base pairs are still overlaped. The highest temperature used in

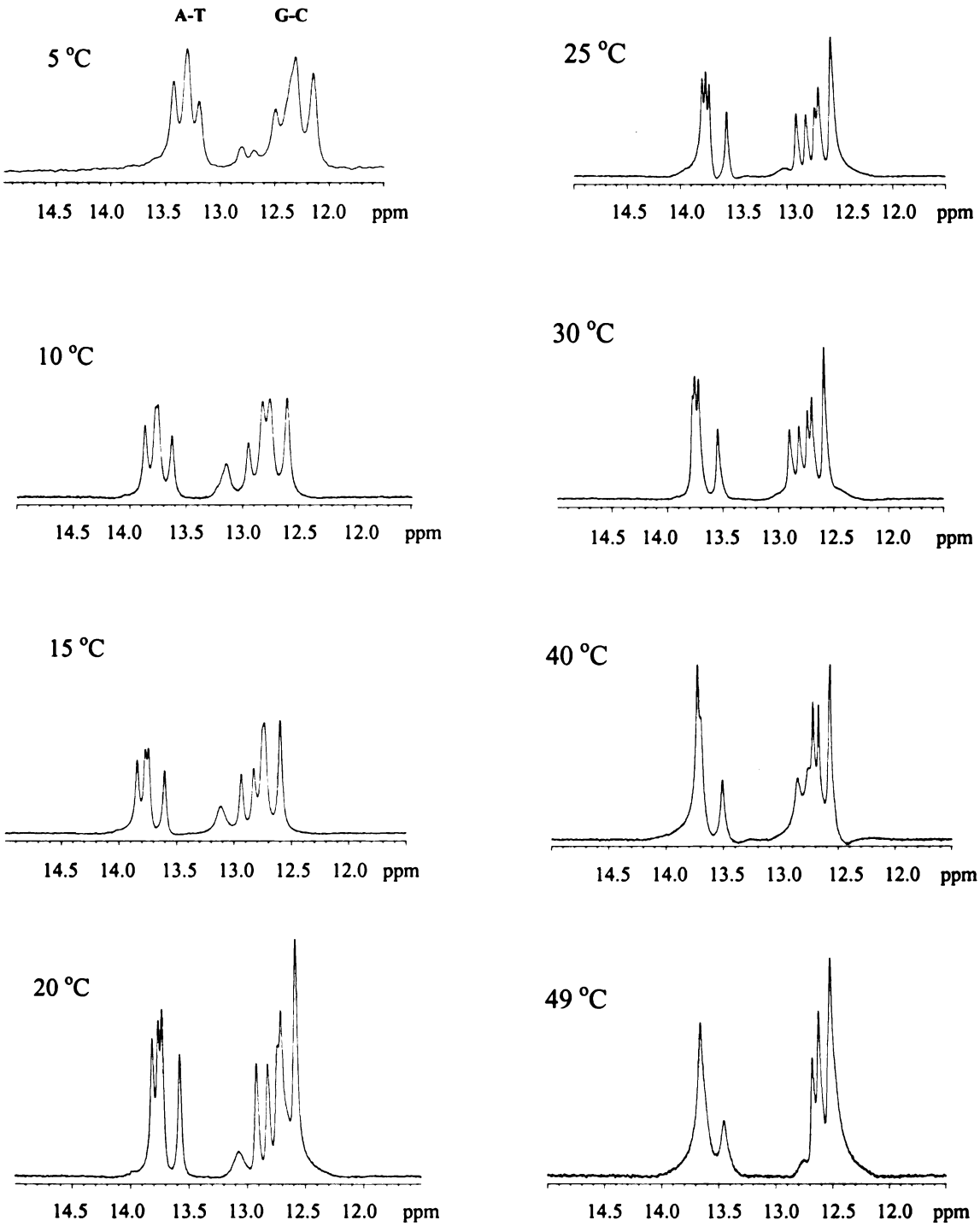

Figure 24. Imino Region of DNA Duplex at Different Temperatures

this experiment was 49 °C, and even at this temperature some of the resonances are still intense. This confirms the high stability of this duplex. For all the experiments, the water resonance was adjusted to the correct chemical shift as the temperature was varied.

In a NOESY spectrum, we can observe the connections between protons that are close in space. The spectrum can be analyzed by dividing it into small regions. Each region will consist of the chemical shifts for a group of protons of the oligonucleotide structure along the horizontal axis (W_1) and the chemical shifts of another group of protons along the vertical axis (W_2). Thus, we can follow, by alternating vertical and horizontal lines, the cross-peaks that represent *inter*nucleotide and *intra*nucleotide connections between different proton groups along the DNA sequence. This procedure is called a NOESY walk. The regions that provide the most information through NOESY walks are the aromatic region (H8 of A and G, H6 of C and T) and the H1' and H3' regions of the sugar residues. The connections between the sugar H1' protons and aromatic H6/H8 protons of C,T/A,G can be observed in Figure 25 where each of the arrows represents a cross-peak in the 2D spectrum.

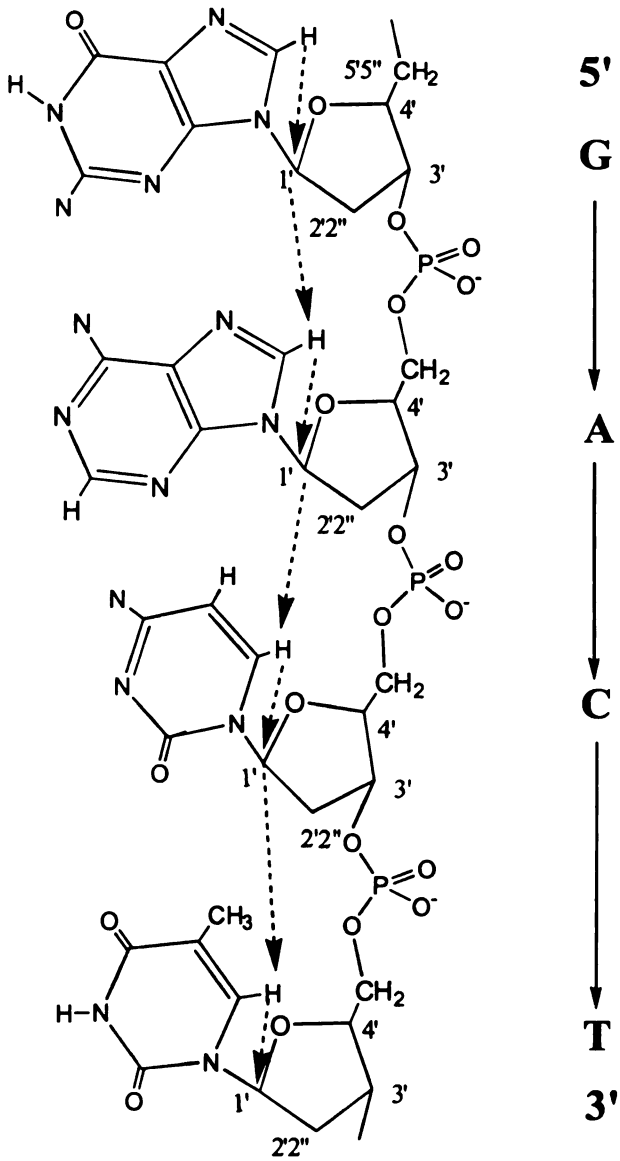

Figure 25. Base-to-H1' NOE Connections

A 2D WATERGATE NOESY spectrum was acquired in 90% H_2O/10% D_2O at 25 °C in order to examine the connections between imino protons. The pulse sequence is the basic NOESY sequence with a WATERGATE pulse sequence inserted after the first 90° pulse. The spectral width was 14500 Hz in F_1 and F_2 dimensions with a mixing time of 250 msec and a recycle delay time of 5 seconds. Each FID was the average of 64 scans using 512 t_1 increments. A total of 2048 complex points out of a total of 4096 real points were used. Data processing was performed by using NMR Pipe (Molecular Simulations Incorporated). This program contains a collection of NMR tools for the UNIX workstation environment It also contains a conversion program that allows for the implementation of processing schemes directly from the spectrometer data format.

During the data processing, solvent subtraction was performed in the time domain. Baseline correction was obtained by using a square polynomial function in the frequency domain. A 0.4 shifted cube cosine bell window was used as the apodization function. Zero-filling was also applied for the next 4096 points. Forward and backward linear prediction (LP) was used for respective prediction and replacement of data at the head and tail of the FID. The full spectrum is presented in Figure 26. By looking at the expanded region of the spectrum that connects the imino-to-imino protons

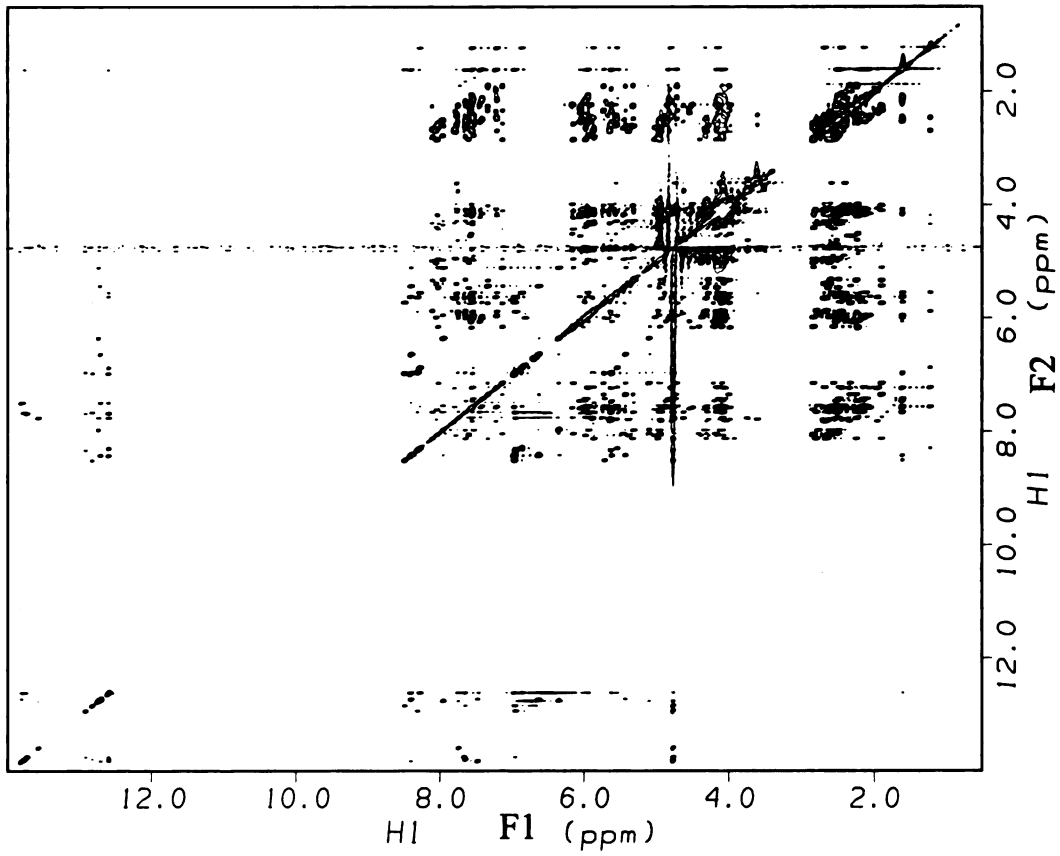

Figure 26. DNA Duplex WATERGATE NOESY Spectrum at 25 °C

in Figure 27, it can be observed that each A-T imino proton is connected to two G-C imino protons, thereby illustrating the communication between hydrogen-bonded imino protons of the duplex.

Following the same reasoning, it can be assumed that the bases of the next lowest intensities will correspond to the bases next to the ends of the duplex. It is also important to note the existence of a complete overlap between C4-G21 and C9-G16 imino protons. Therefore, these assignments could only be made by combining this portion of the spectrum with regions connecting the aromatic and H1' protons and also with the amino-imino connections. As stated before, the ends were not observable and the least intense peaks corresponded to G23-C2 and G14-C11 base pairs.

1D and 2D NOESY ^{1}H NMR spectra in D_2O at 25 °C were performed for the same sample using the Varian 600 MHz spectrometer. The sample was concentrated to dryness, dissolved in 99.9% D_2O and concentrated again *in vacuo*. This process was repeated three times with the sample being back-filled with argon each time in order to reduce exposure to atmospheric H_2O as much as possible. Once again, a Shigemi NMR tube was used following the same procedure for the loading of the sample and elimination of the air bubble enclosed between the glass plugs. A 1D ^{1}H NMR spectrum of this sample is depicted in Figure 28.

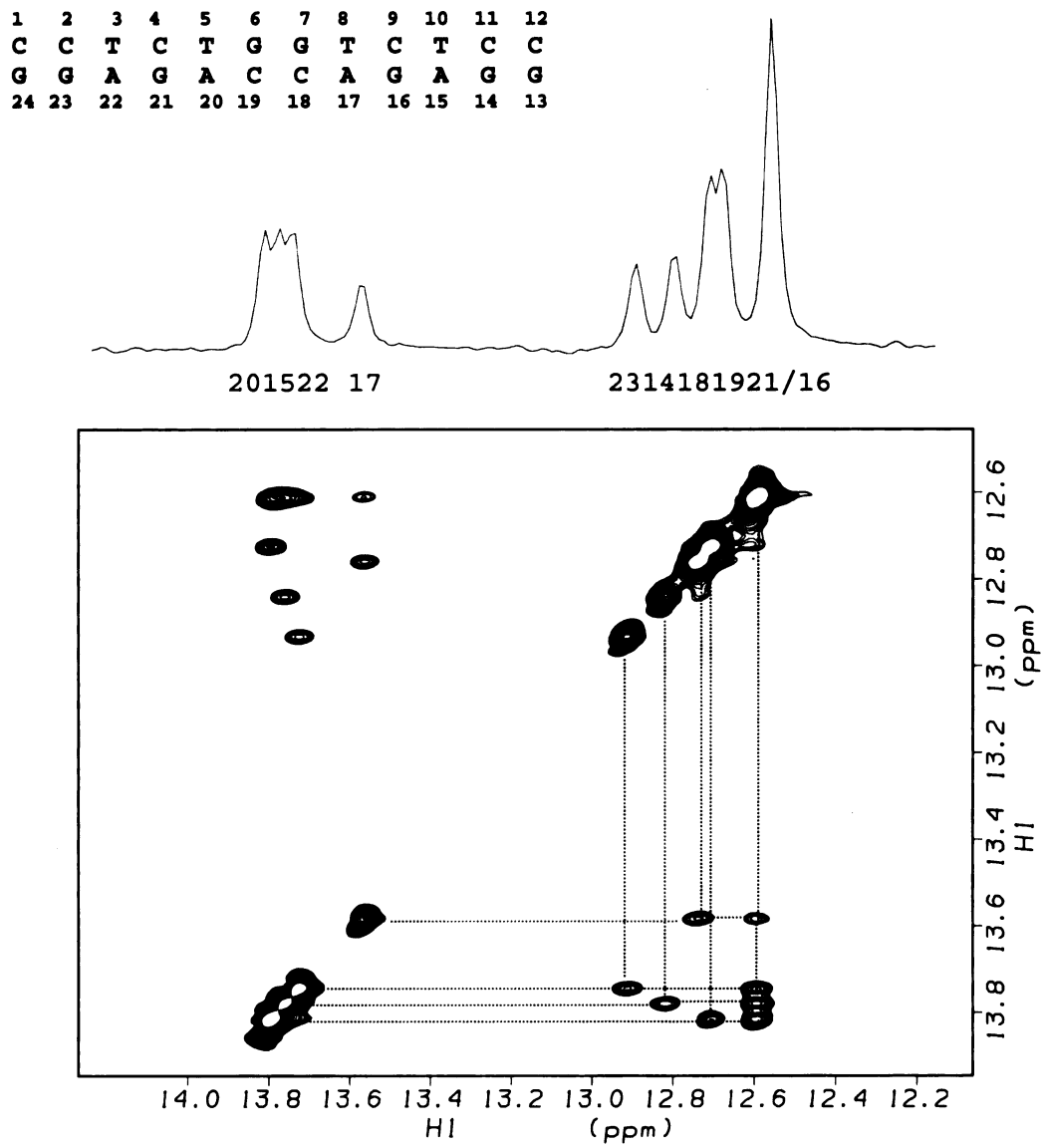

Figure 27. 2D Imino Region of DNA Duplex

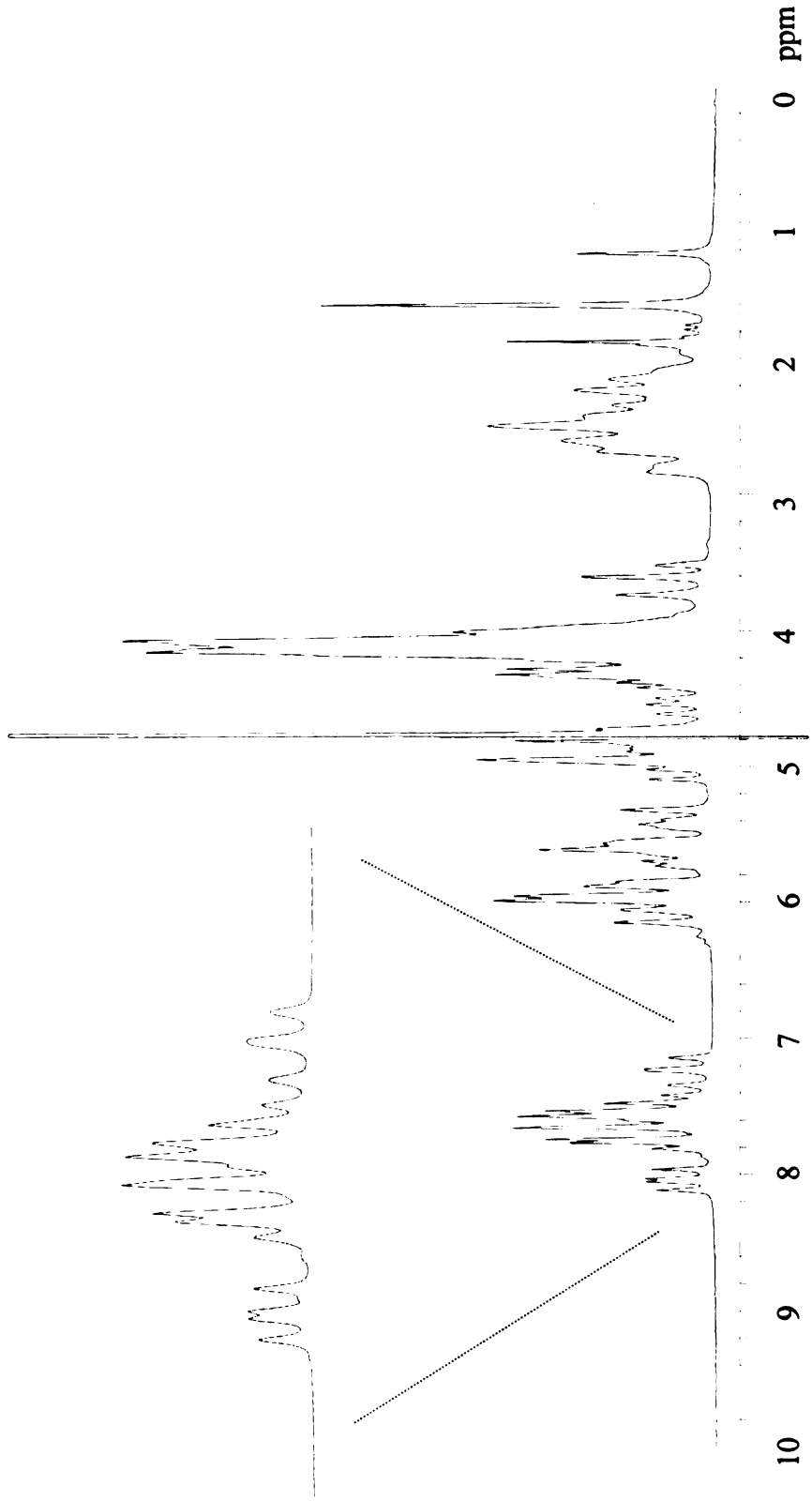

Figure 28. DNA 12-mer ^{1}H NMR Spectrum in 99%D_2O at 25 °C

An inversion recovery experiment was first performed in order to obtain the T_1 relaxation values for the AH2 protons. This allows for the selection of the best recycle delay time, d1, for obtaining a better 2D data. The relaxation time T_1 observed for these protons was 4 sec which is relatively long compared to the values for other protons, e.g. the H8's which exhibit values between 1-2 sec. Therefore the delay time was set to three times this value, which represents a compromise between obtaining fully relaxed signals before each cycle, and increasing the amount of time required for the experiment. Along with T_1 experiments, measurements of transverse relaxation time (T_2) were performed. With these two measurements, the correlation time τ_c of the DNA duplex that describes the overall tumbling rate of the molecule can be calculated by using an equation that relates the T_1 and T_2 relaxation times which were measured experimentally for individual protons.[34]

$\tau_c = (2/\omega)[T_1/3T_2]^{1/2}$ where ω is the Larmor frequency

The correlation time was calculated for the base protons AH8. The results are presented in Table 2 with an average τ_c value of 2.19 ± 0.03 ns.

Table 2. DNA 12mer : Relaxation and Calculated Correlation Times for AH8 Protons

	T_1(s)	T_2(s)	τ_c x10^{-9} (s^{-1})
A20H8	2.358	0.0666	2.188
A15H8	2.427	0.0695	2.173
A17H8	2.431	0.0707	2.156
A22H8	2.451	0.0670	2.223

It is important to note that although the calculation of the correlation time was made with only a few protons, the reliability of the value obtained is acceptable since these protons are isolated in the spectrum without interference from coupling to other protons. This fact allows for an accurate measurement of their relaxation times to be obtained.

The NOESY experiment was set with the same parameters used for the sample in H_2O at 25 °C. The processing parameters were similar to those used in earlier experiments, but in this case a polynomial cube function in the frequency domain was used for baseline correction and only forward LP was needed. The full spectrum is shown in Figure 29.

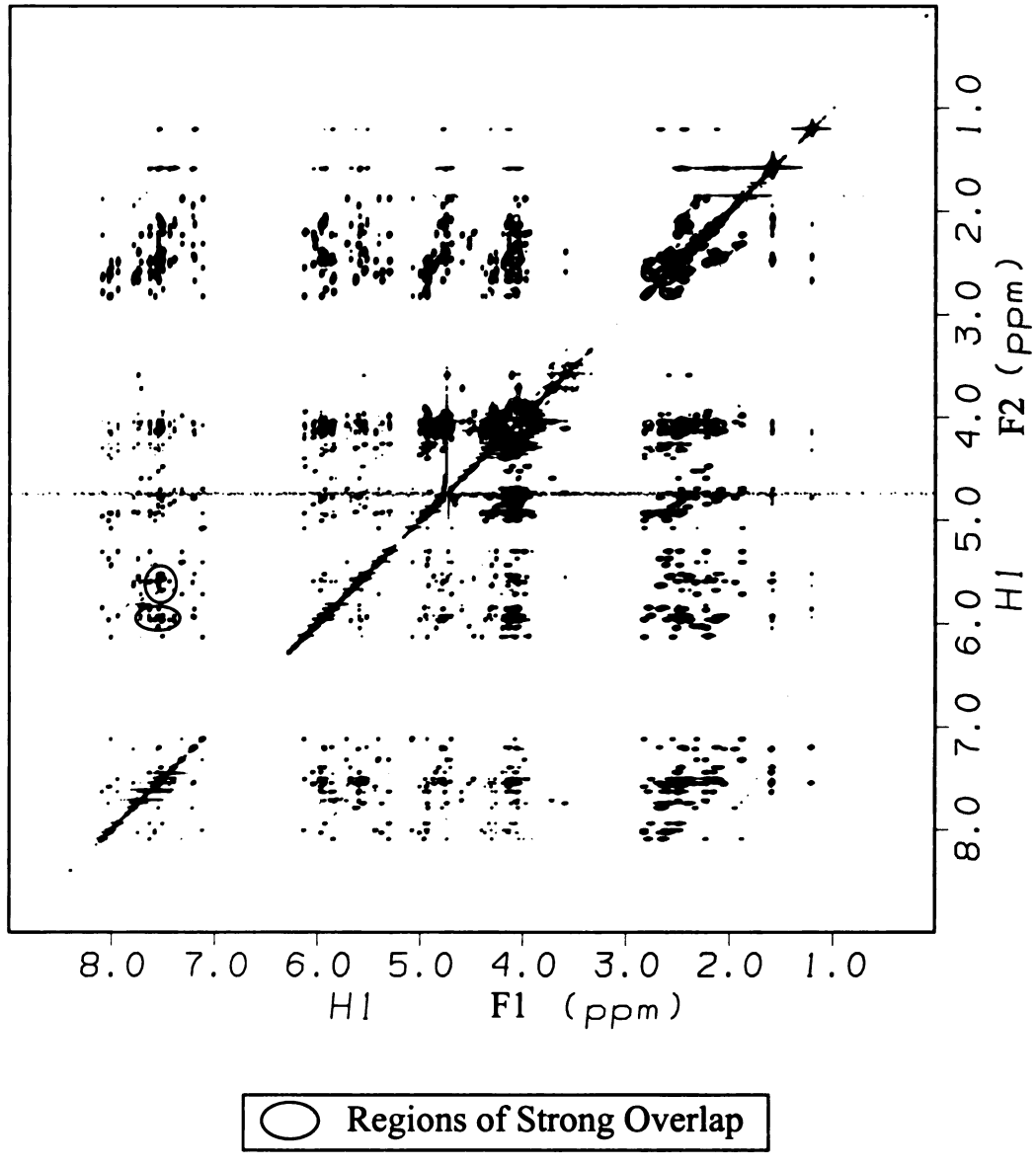

Figure 29. DNA Duplex NOESY Spectrum in 99% D_2O at 25 °C

The assignment process was performed following an established protocol.[35] The assignments were initiated in the base to H1' region. The AH8 protons were easily recognized by their shape and chemical shifts. They were easily differentiated from AH2 protons because the latter are sharper and, in most cases, they are associated with some T_1 noise due to their slow relaxation rates. This T_1 noise is represented by bands of random fluctuations running parallel to the F_1 dimension at the position of strong and sharp diagonal peaks which tend to distort the spectra. A problem observed during the assignment procedure was the presence of regions in the spectrum with severe overlap. Some of the cross-peaks coincide in the same chemical shift region rendering them undistinguishable. Due to this fact, 1D experiments at different temperatures were performed in order to obtain better resolution of the overlapping resonances to continue the assignments and confirm the ones already made. The temperature selected was 30 °C due to the better separation and sharper line-widths for the resonances. A NOESY experiment was performed at this new temperature eliminating the majority of overlapped regions. The 1D and 2D spectra obtained at 30 °C are presented in Figures 30 and 31 respectively.

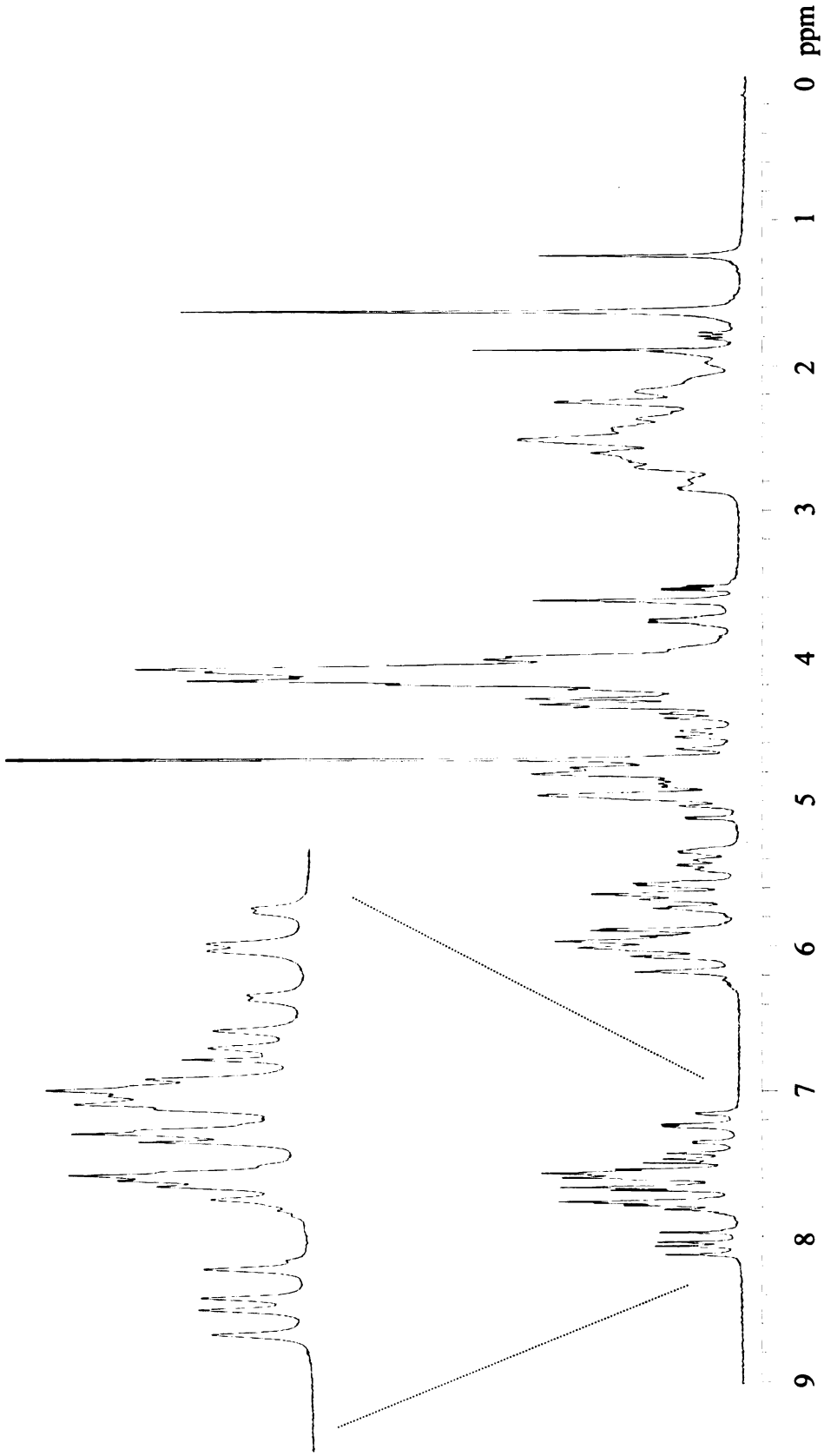

Figure 30. DNA 12-mer ^{1}H NMR Spectrum in 99% D_2O at 30 °C

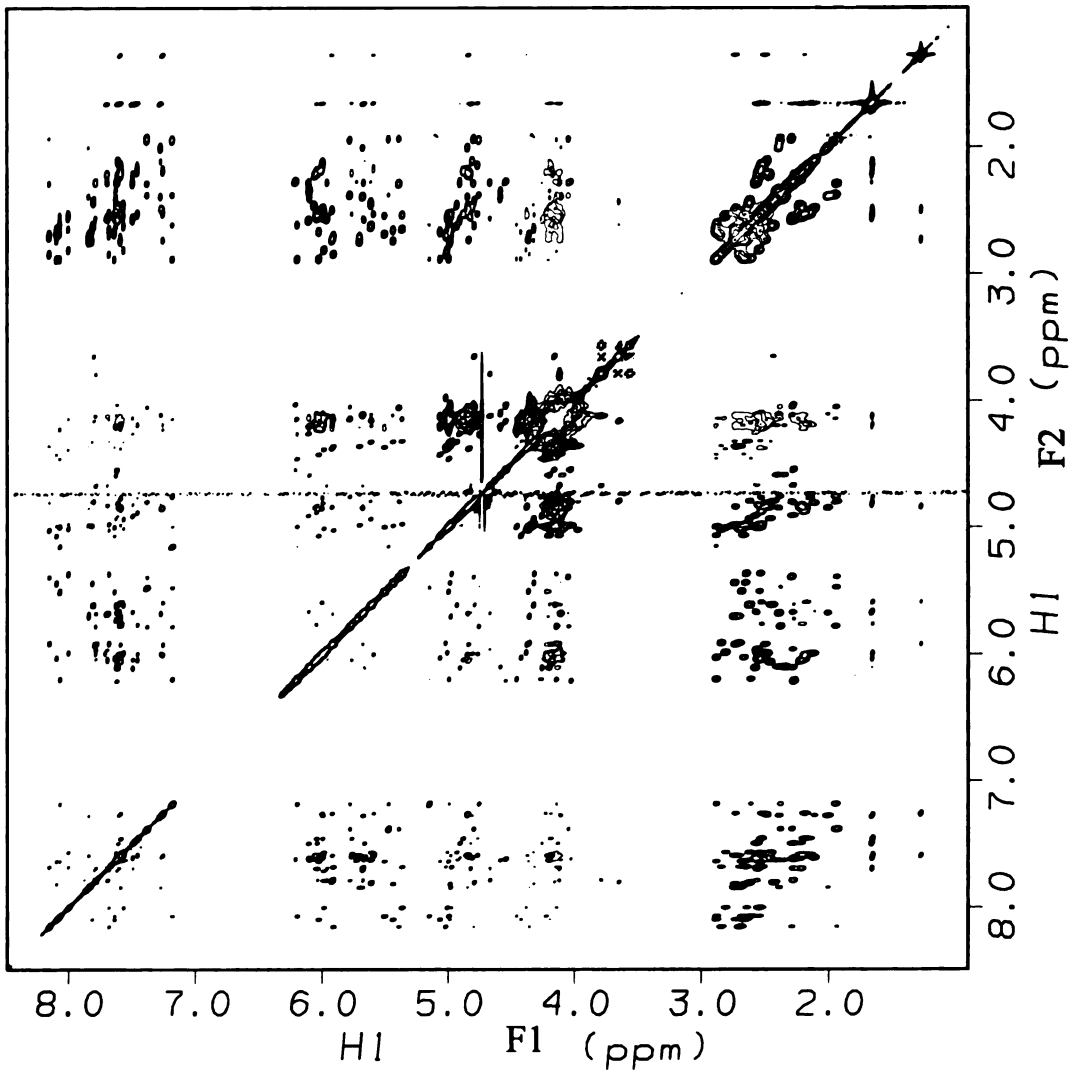

Figure 31. DNA Duplex NOESY Spectrum in 99% D_2O at 30 °C

A TOCSY experiment was also performed at the same temperature. The spectrum is presented in Figure 32. This experiment is designed to locate the H5-H6 scalar coupling cross-peaks of the C residues. Furthermore, some of the directly coupled proton resonances were confirmed from the 2Q COSY spectrum taken at 25 °C (Figure 33). This spectrum, together with the 2D NOESY data, led to the observation that there were two consecutive C bases connected to each other that were connected to A bases as well. From this information, these residues were assigned to the C residues located in the middle of one of the strands. For a standard B form DNA oligonucleotide, there are many possible *inter*nucleotide and *intra*nucleotide proton distances. Some of the distances that were useful for our initial assignments are presented in Table 3.[36]

Table 3. Base-to-Base and Base-to-H1' Intra and Interresidue Distances

5' -> 3'	Intra-residue Dist. (Å)	Inter-residue Dist. (Å)
H8 - H1'	3.9	7.7
H1'- H8		2.8
H5 – H6		5.0
H6 – H5		3.7

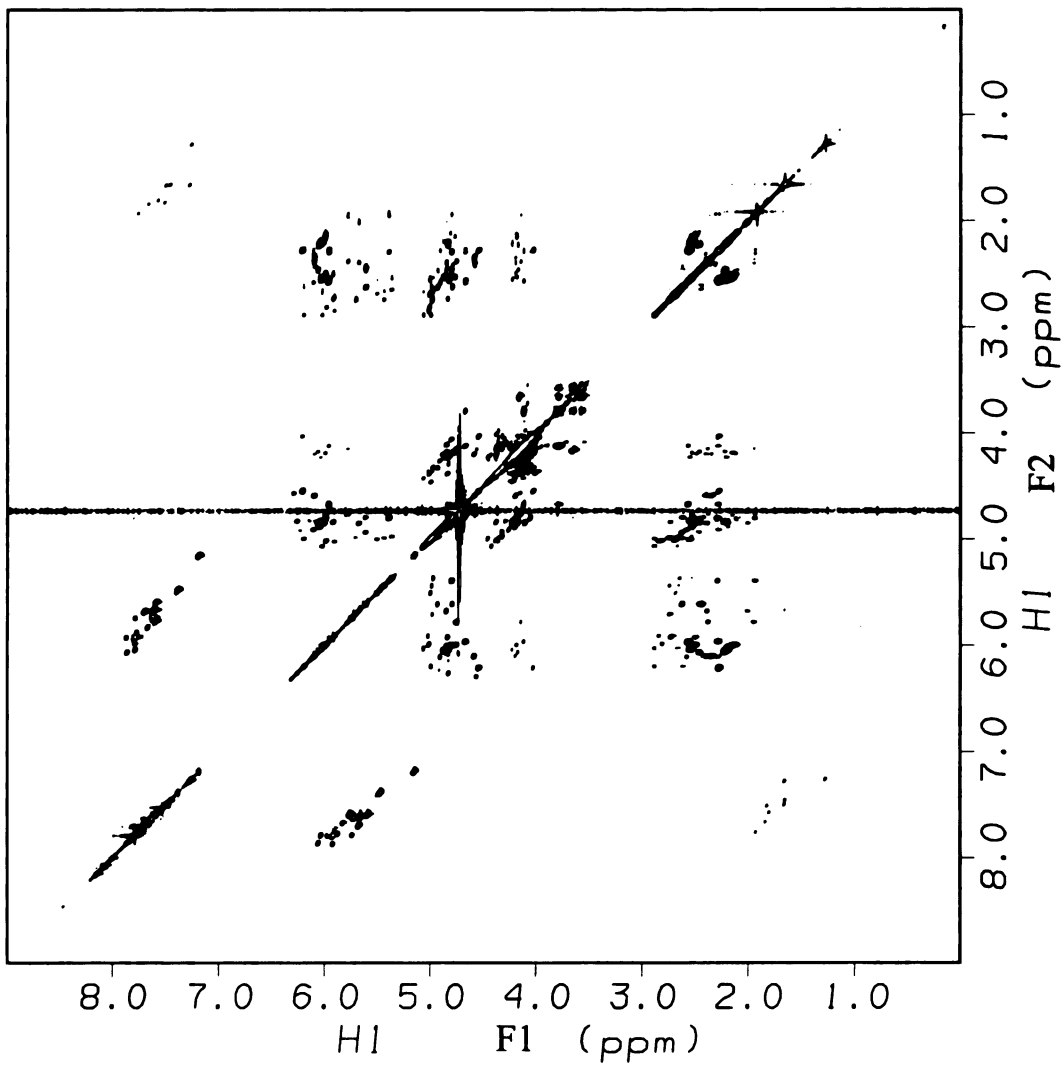

Figure 32. DNA Duplex TOCSY Spectrum in 99% D_2O at 30 °C

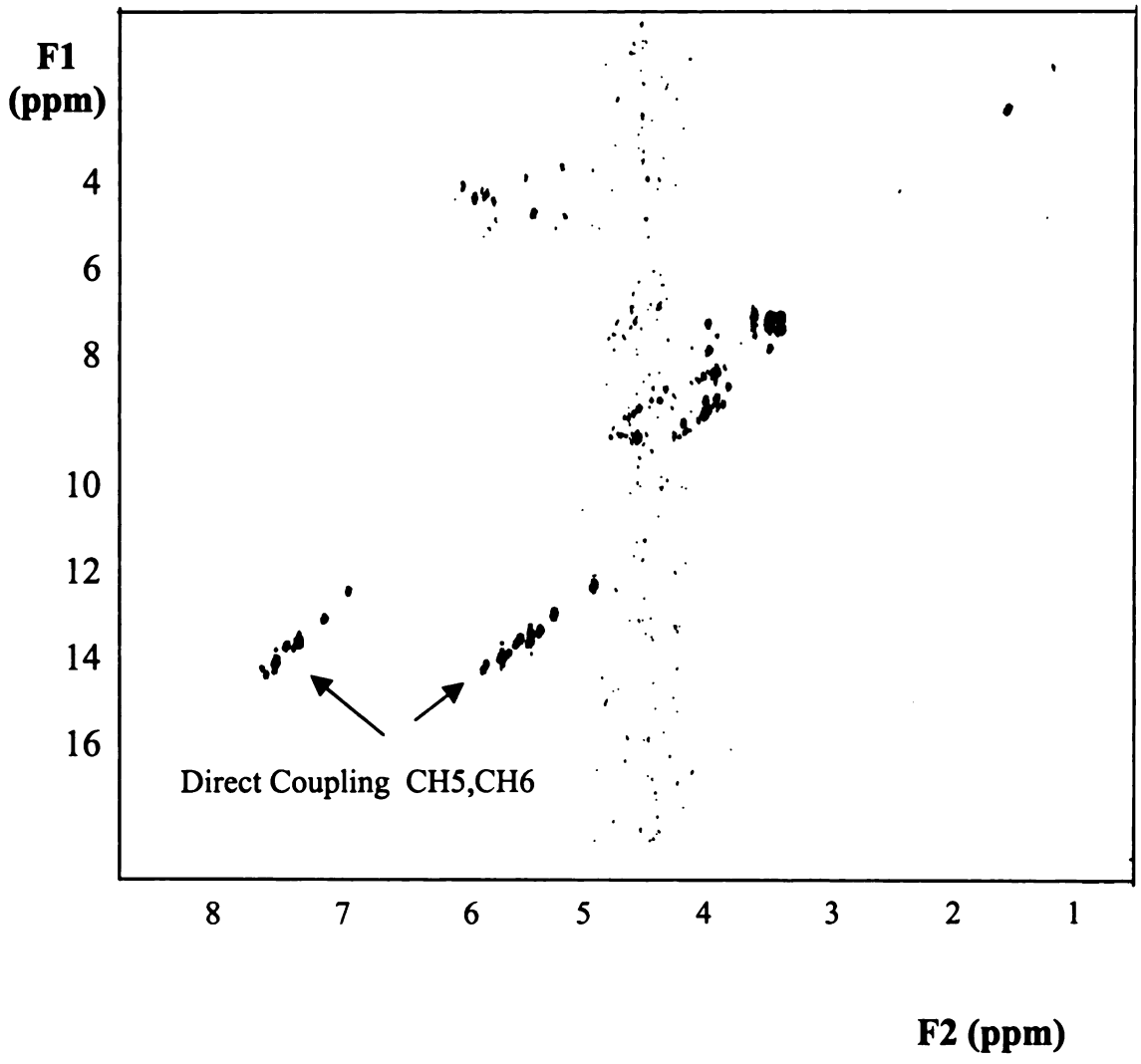

Figure 33. 2Q COSY Spectrum of DNA Duplex at 25 °C

From the information in Table 3, one can observe that the cross-peak that represents a distance between the aromatic proton (H6/H8) and the sugar proton H1' within the same residue is less intense than the cross-peak representing the same distance between consecutive residues. This observation is what one would expect for the B form of DNA.

Furthermore, from the internucleotide distances between H6 and H5 of the C bases, the distinction between C18 and C19 was possible, since in the B form of DNA, the cross-peaks that correspond to this distance going from 5' to 3' are more intense than those corresponding to the distance going from 3' to 5'. Therefore, only one cross-peak that connects these two base protons is observed. From this starting point, the NOESY walk was continued until both ends were located. The intensity pattern agrees for most of the assignments with the intensity of the cross-peaks assigned as *intra* or *inter*nucleotide connections. The expanded version corresponding to this region can be observed in Figure 34.

The assignment process was continued with the region that corresponds to the connections between the sugar protons H1' and H3' (Figure 35). During these assignments the chemical shifts for each H1' protons were confirmed by examining the region already assigned. The aromatic-aromatic region was assigned as well.

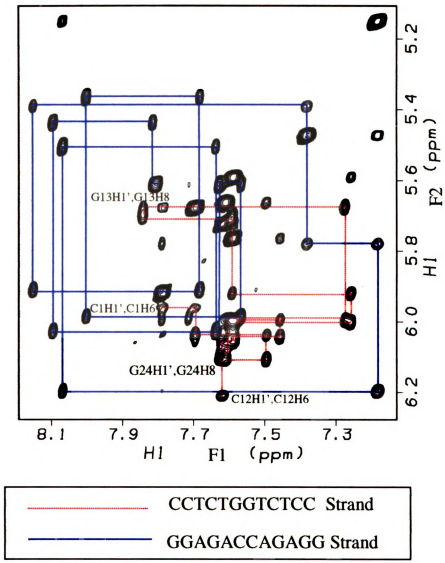

Figure 34. Base-to-H1' NOESY Walk

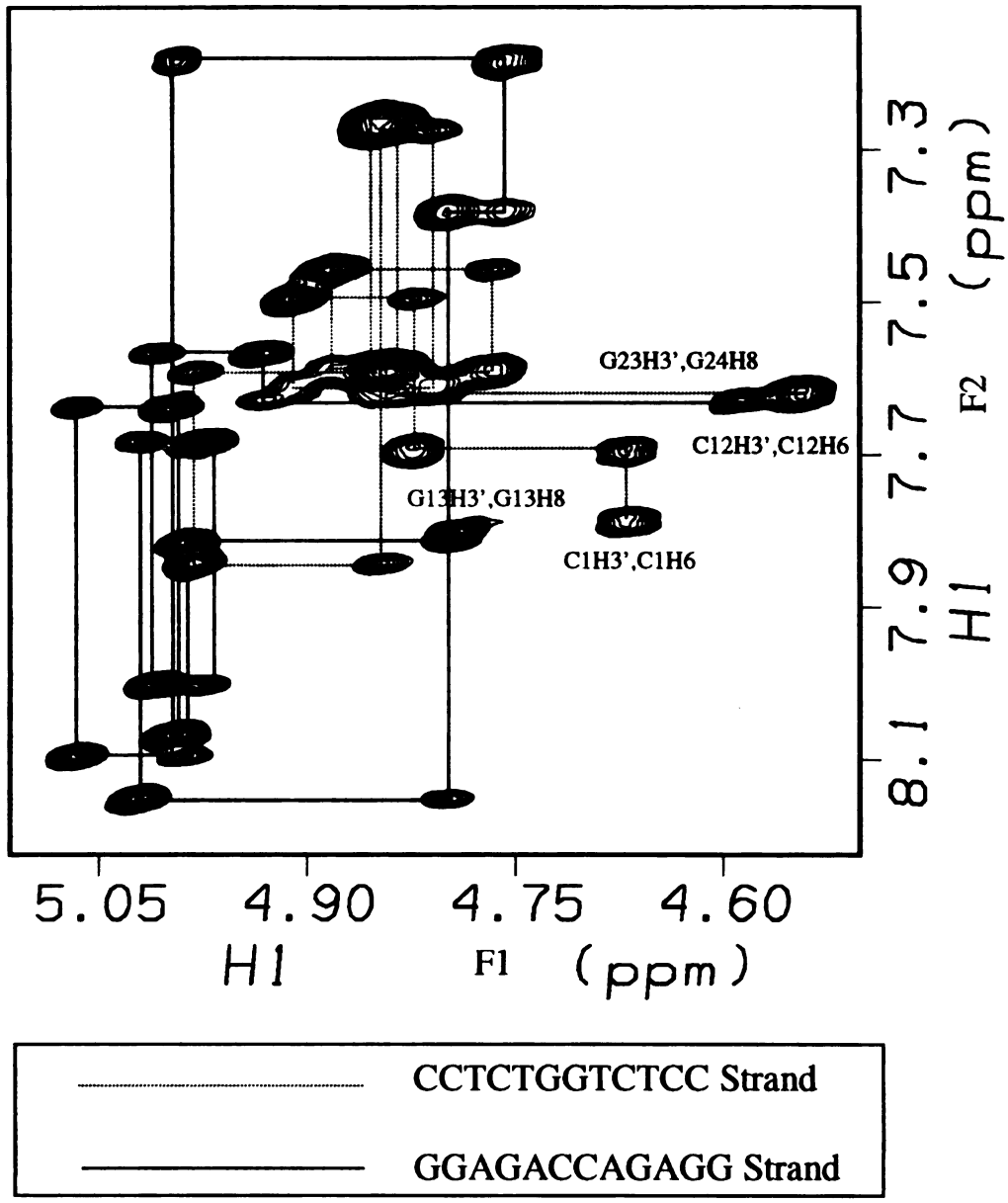

Figure 35. H3'-to-Base NOESY Walk

D. Reaction of the DNA Dodecanucleotide with Dirhodium Acetate Complex

The metallated DNA oligomer was synthesized by reacting the purified - GG- 12-mer with the compound $[Rh_2(O_2CCH_3)_2(CH_3CN)_6][BF_4]_2$ in a 1:1 ratio. The ^1H NMR spectrum of this starting material in D_2O is presented in Figure 36. Once the purple solution of the compound is added to the DNA sample, the color immediately changes to bright orange. The reaction was continued by incubation in a thermocycle at 70 °C for 72 hours, and small aliquots of the reaction mixture taken at regular intervals were injected into an HPLC to monitor the progress of the reaction. This method revealed that the reaction had gone to completion in ~72 hours. The color of the solution after incubation is dark green. Once this product was purified, the complementary strand was added to form the duplex.

The purification process was performed in the same manner as for the native DNA oligonucleotide by HPLC chromatography using acetate buffers in the following concentrations:

Eluant A : 0.02 M NaOAc , 20% CH_3CN

Eluant B : 0.02 M NaOAC, 20% CH_3CN , 1.2 M KCl

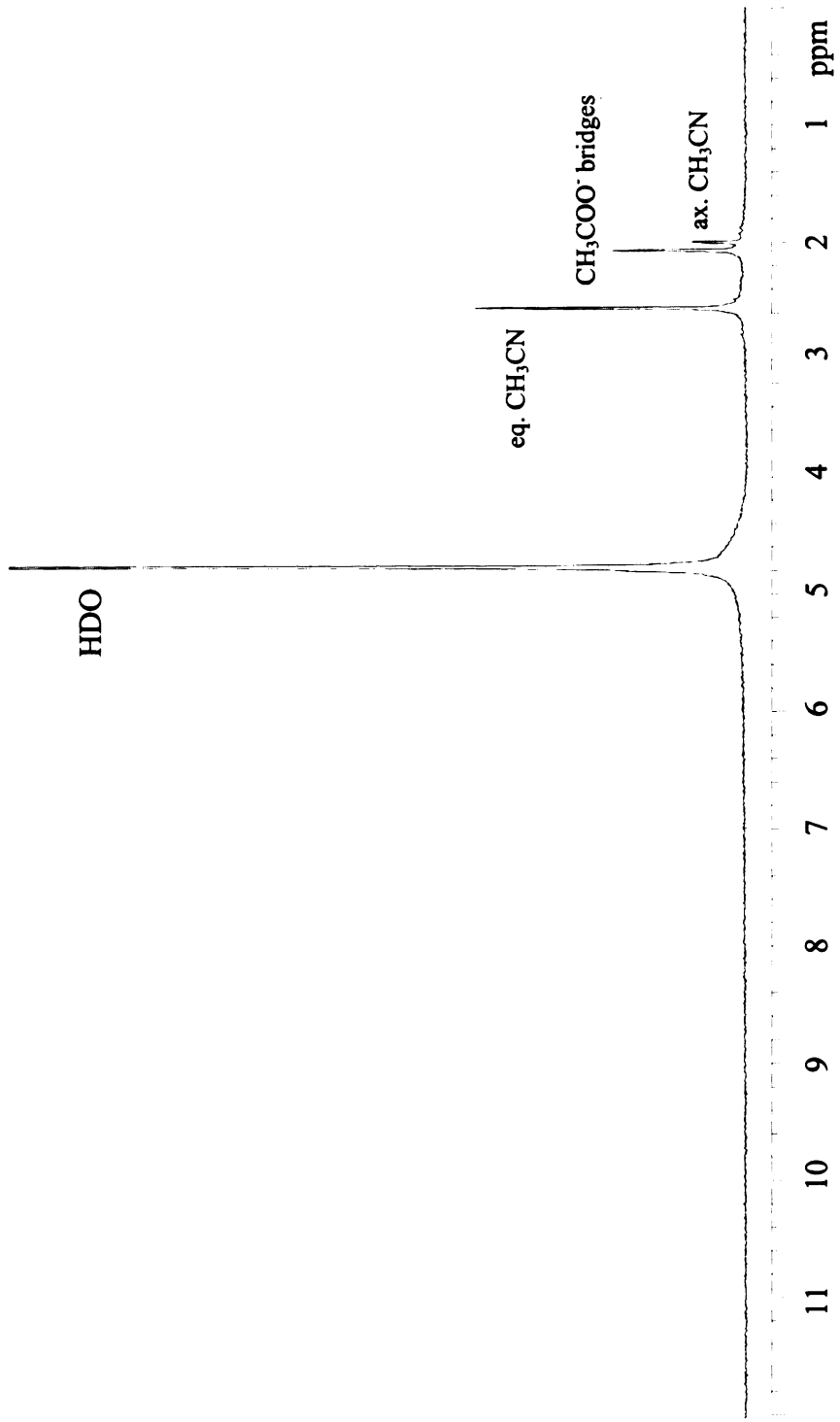

Figure 36. ^{1}H NMR Spectrum of $[Rh_2(O_2CCH_3)_2(CH_3CN)_6][BF_4]_2$ in D_2O

The gradient that was used is as follows:

Time(min)	%A	%B	Flow Rate (mL/min)
0	100	0	4
5	70	30	4
65	60	40	4
70	0	100	4
75	0	100	4
80	100	0	4

The ionic exchange column was also used for this particular separation, but the product did not elute from the column until eluant B was in high percentage in the elution mixture (86%). This may be due to steric factors that begin to play an important role because the overall shape of the DNA strand is affected by metal binding. The detection of the adduct was possible by using a diode-array UV visible detector. The DNA absorbance was detected at 260 nm while the Rh_2 chromophore was detected at 365 nm. The sensitivity of the Rh detector was increased ten times more than for the DNA due to the low extintion coefficient for the metal-based transition (ε = 46 M^{-1} cm^{-1}) at 365 nm compared to the extintion coefficient of DNA at 260 nm ($\varepsilon = 1.18 \times 10^4 M^{-1}cm^{-1}$). The chromatogram is presented in Figure 37.

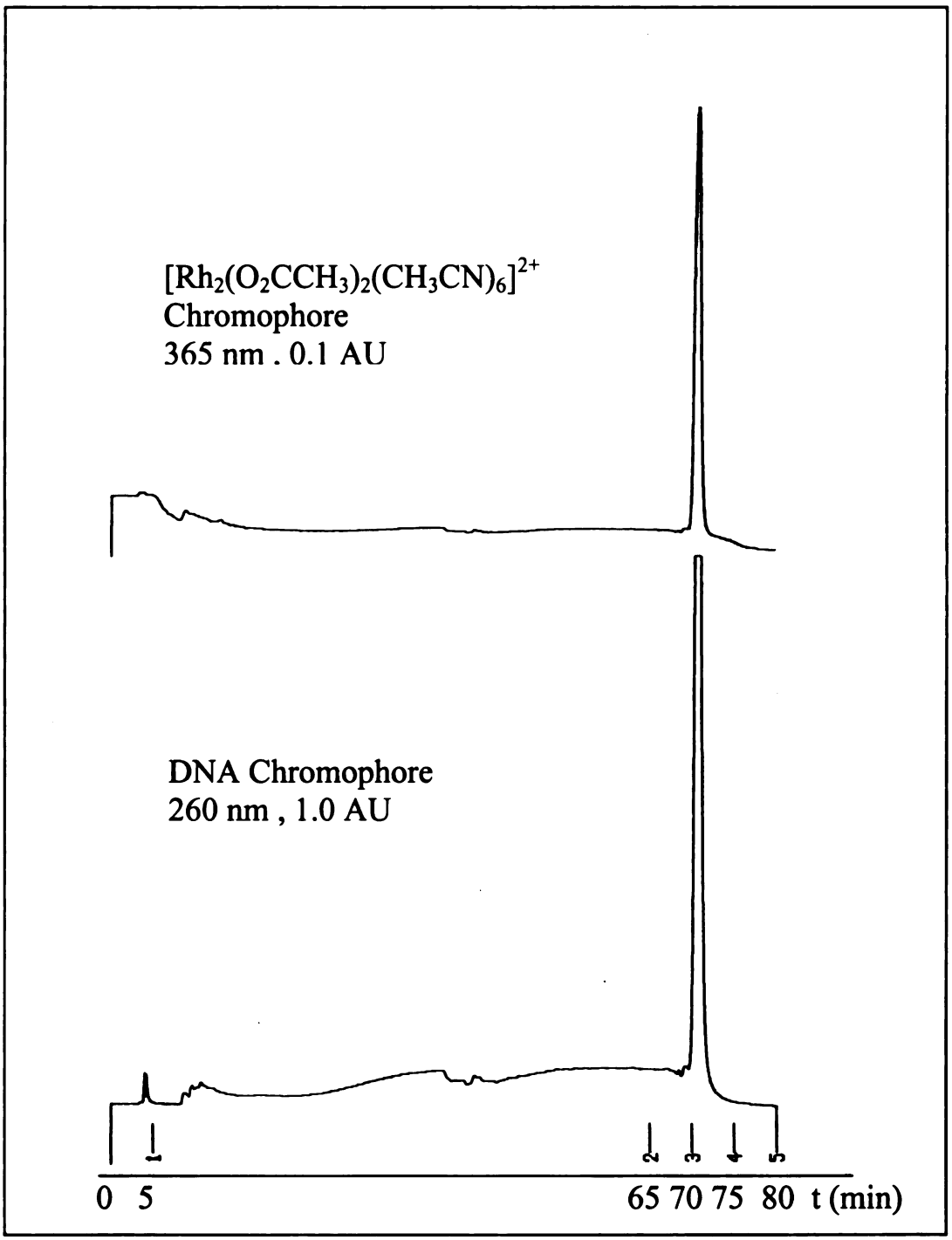

Figure 37. HPLC Chromatogram of Rh_2-DNA Adduct

E. ^{1}H NMR Analysis of Rh_2-DNA Adduct

The NMR analysis of the dirhodium-DNA adduct was performed on a sample whose concentration was 1.3 mM. Buffer solution in the same concentration used for the unmetallated duplex (10 mM Na_2HPO_4/NaH_2PO_4, 50 mM NaCl and 0.1 mM $NaC_2H_6AsO_{2)}$) was added to a final volume of 0.250 mL in a Shigemi tube.

The experiments were initiated by measuring 1D spectra of the imino region in 90% H_2O using the binomial method. Experiments at different temperatures were performed to observe variations in chemical shifts or resonance intensities as the duplex was denatured (Figure 38). By examining the spectra it is obvious that after metallation and addition of the complementary strand, the duplex has formed, since the imino protons are observed. The spectra reveal some changes of the resonances as a result of metallation, for example at 25 °C one of the A-T imino protons is no longer observed. This proton corresponds to the A20-T3 base pair which is next to the metallation site. Furthermore, the temperature range over which the metallated duplex is stabilized is dramatically different as compared to the native oligonucleotide. The duplex is practically denatured at 49 °C while in the native duplex some resonances can still be observed at this temperature.

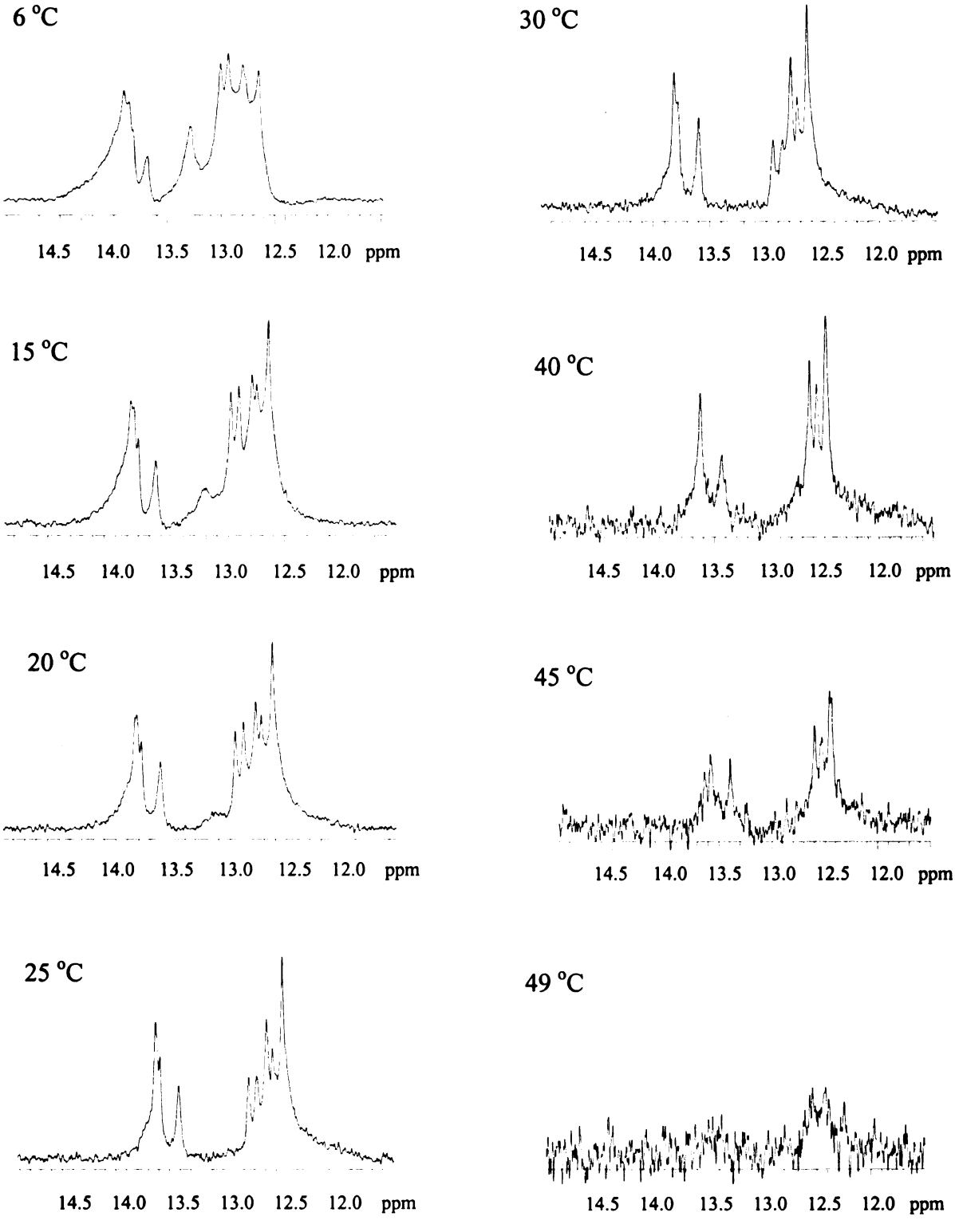

Figure 38. Imino Region of Rh_2-DNA Adduct at Different Temperatures

A 1D ^{1}H NMR spectrum of the metallated DNA product in 99% D_2O was measured at 30 °C which was the temperature used for the native DNA 12-mer (Figure 39), and the residual HDO resonance was suppressed. A very intense resonance at 1.8 ppm was observed which corresponds to the acetate group of the metal compound.

Correlation time calculations were also performed following the same procedure used for the unmetallated DNA 12-mer. The results are presented in Table 4 with an average value of τ_c of 1.10 ± 0.05 ns.

Table 4. Rh_2-DNA Adduct : Relaxation and Calculated Correlation Times for AH8 Protons

	T_1(s)	T_2(s)	τ_c x10^{-9} (s^{-1})
A20H8	1.787	0.1999	1.099
A15H8	1.882	0.1976	1.134
A17H8	1.664	0.1773	1.132
A22H8	1.612	0.2023	1.038

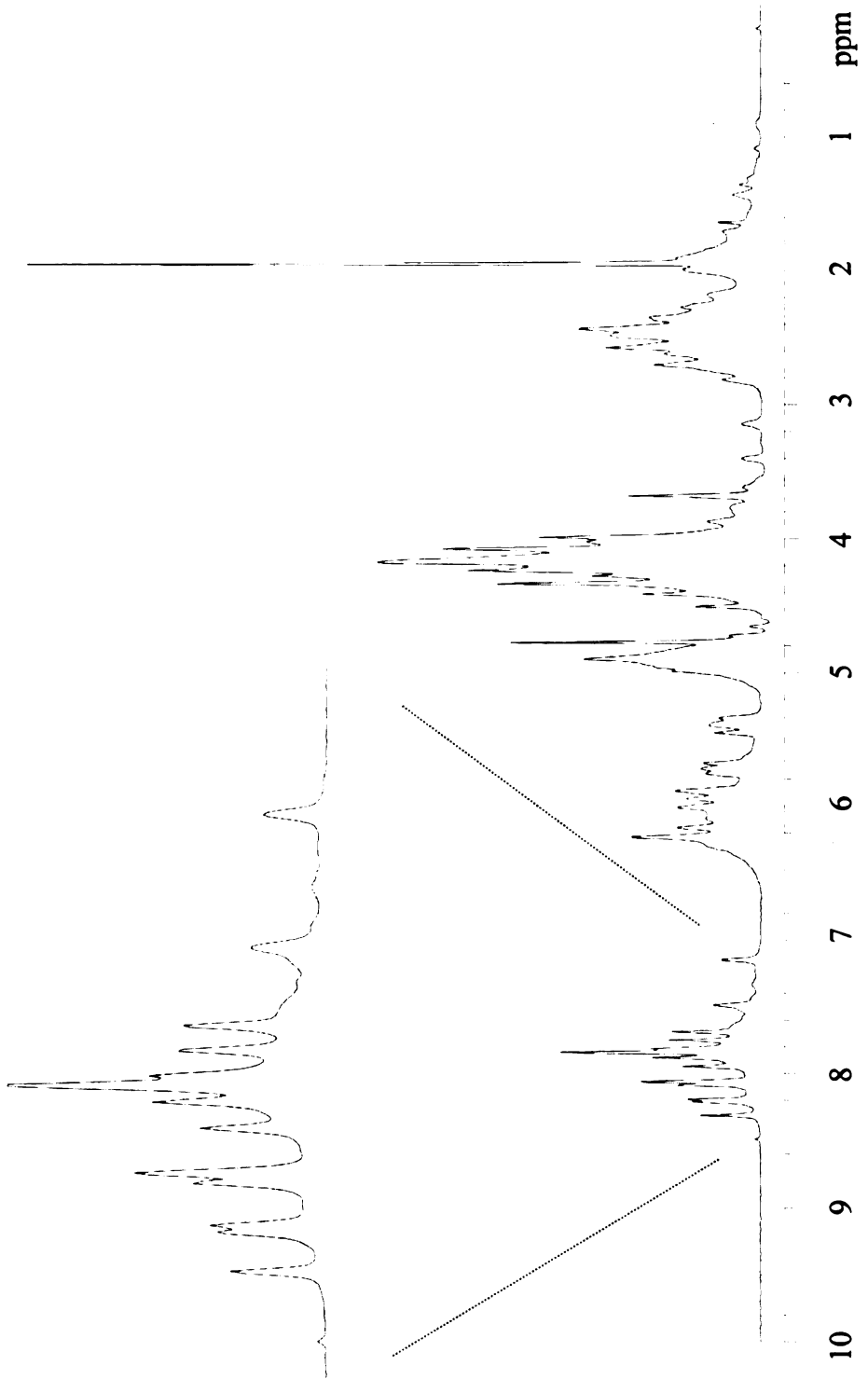

Figure 39. ^{1}H NMR Spectrum of the Rh_2-DNA Adduct in 99% D_2O at 30 °C

The 1D spectrum clearly shows the distortions experienced by the DNA duplex upon metallation. Regarding chemical shifts, differences can be observed in the entire spectrum. In the aromatic region, the resonances of the C residues in the middle of the complementary strand have shifted downfield for C19H6 and upfield for C18H6. The methyl groups of the T residues are not observed, most likely because of shifting of these groups and subsequent overlap with the methyl of the acetate groups. Most of the resonances of the GG strand are not observed which implies strong instability of the duplex as a consequence of metal binding.

Another important point is the correlation time value which is also indicative of the severe effects on the overall conformation of the duplex caused by the binding of the metal complex. This value has decreased considerably compared to the native DNA oligonucleotide, implying a distortion that favors a rapid tumbling of the molecule in solution. Although the value of τ_c has not been calculated for a large number of protons of the biomolecule, it represents a measurable comparison between unmetallated and metallated duplexes since we are taking into consideration the same number and type of protons for the calculation.

After acquiring a 2D NOESY spectrum of this sample at the same temperature, namely 30 °C, the instability of the adduct was confirmed (Figure 40). Chemical exchange effects could be very strong if we consider that according to the imino proton resonances, the melting or denaturing point of the duplex is around 45 °C. Furthermore, by comparing 2D NOESY spectra of metallated and non-metallated duplexes at the same temperature, it is obvious that the line broadening has increased in such a manner that the splitting of the resonances corresponding to C18H6 coupled to C18H5 at 7.18 ppm has been eliminated due to line-broadening. The same phenomenon is observed for the C19 residue as well.

It was decided at this point to decrease the temperature and to measure the 2D spectrum at 20 °C. At this temperature, sharper and more well-resolved resonances were obtained (Figure 41). In the 2D NOESY spectrum measured at 20 °C, severe line broadening was also observed (Figure 42). Focusing specifically on the base-to-H1' region of this spectrum (Figure 43), the cross-peaks corresponding to the non-metallated strand are clearly observed. However the metallated strand cross-peaks coalesce in a region between 7.5 and 8.0 ppm. During chemical exchange, if an ensemble of spins is precessing at a certain frequency, and then some of the spins briefly exchange into another environment with a different

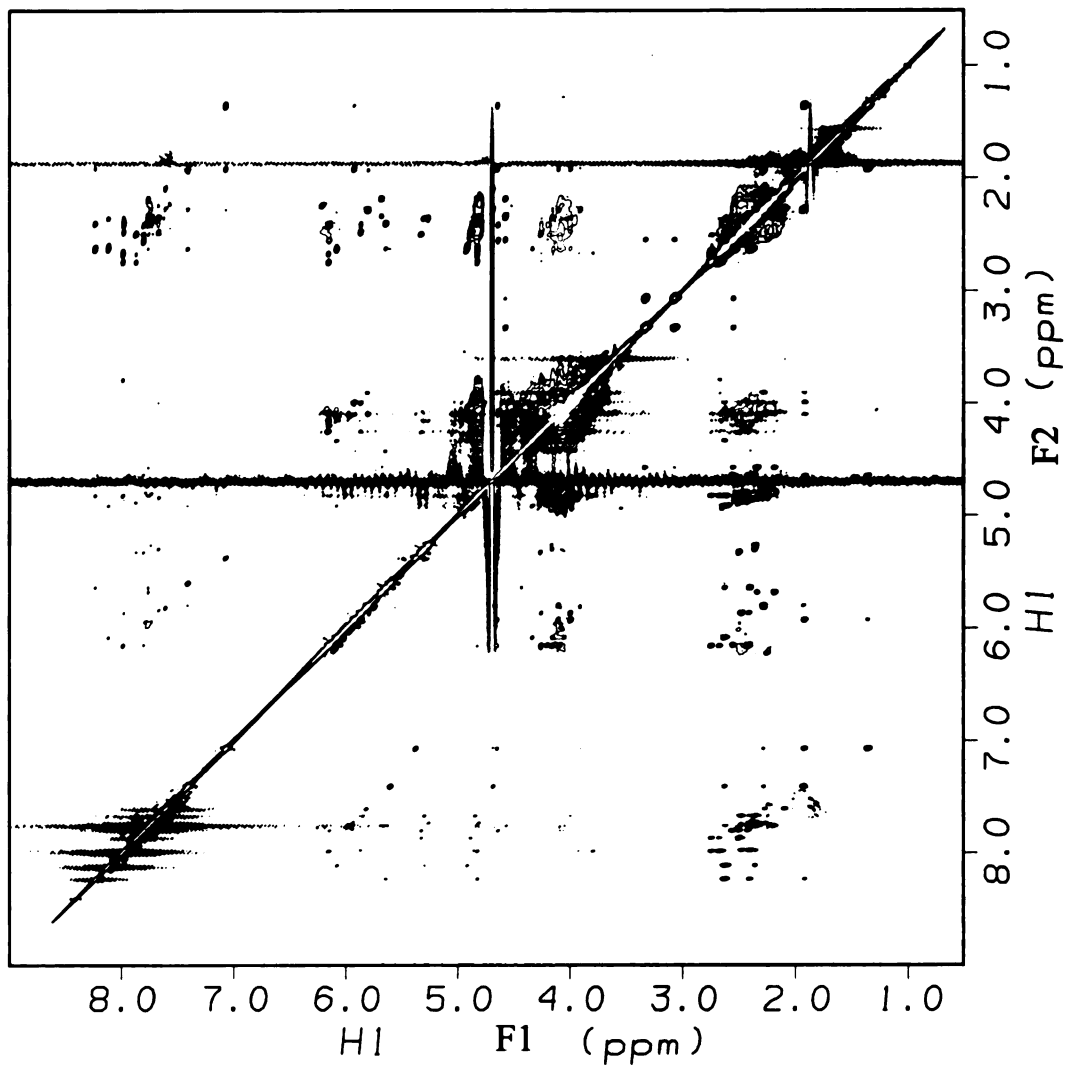

Figure 40. Rh_2-DNA Adduct NOESY Spectrum in 99% D_2O at 30 °C

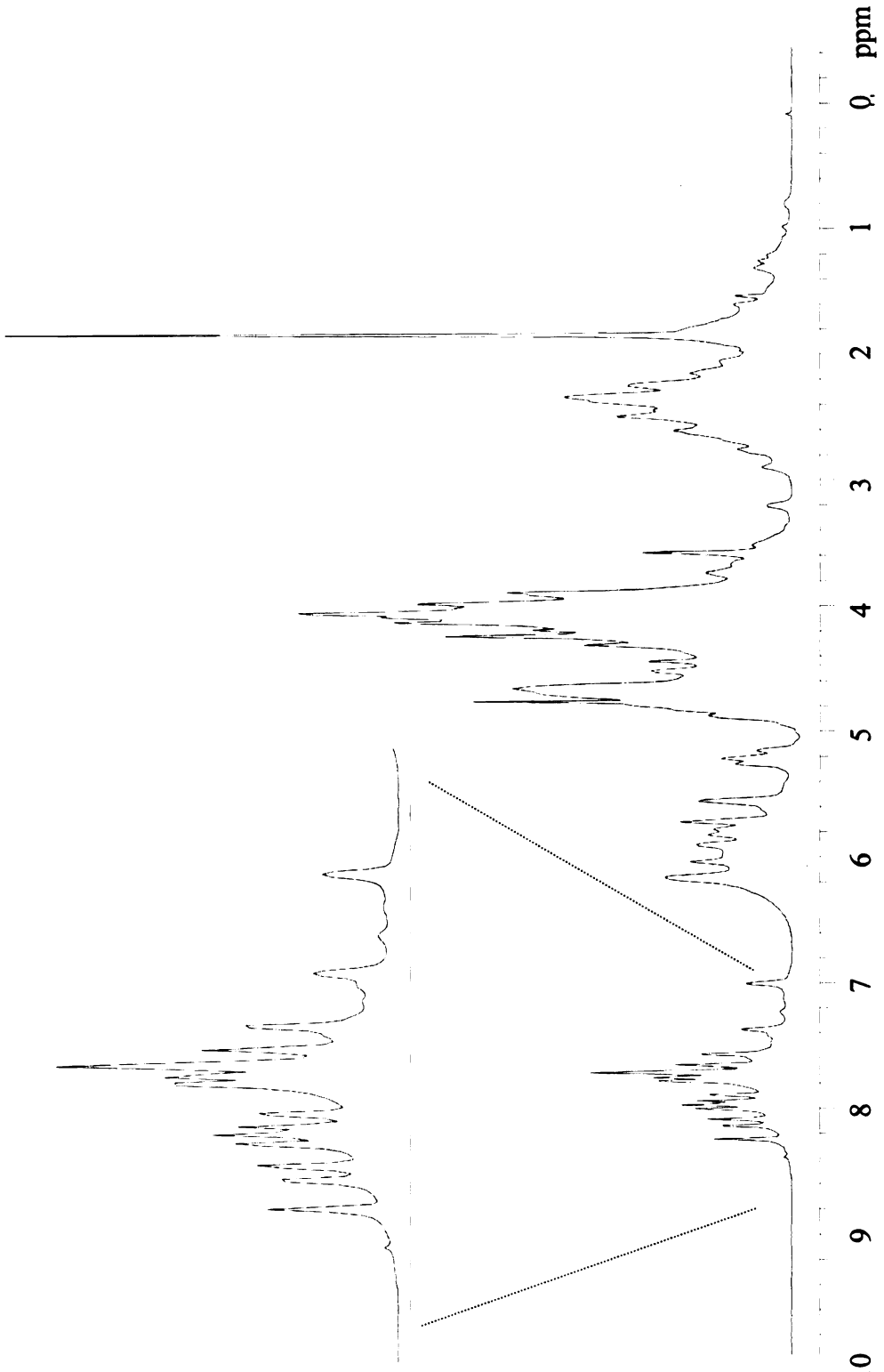

Figure 41. Rh_2-DNA Adduct ^1H NMR Spectrum in 99% D_2O at 20 °C

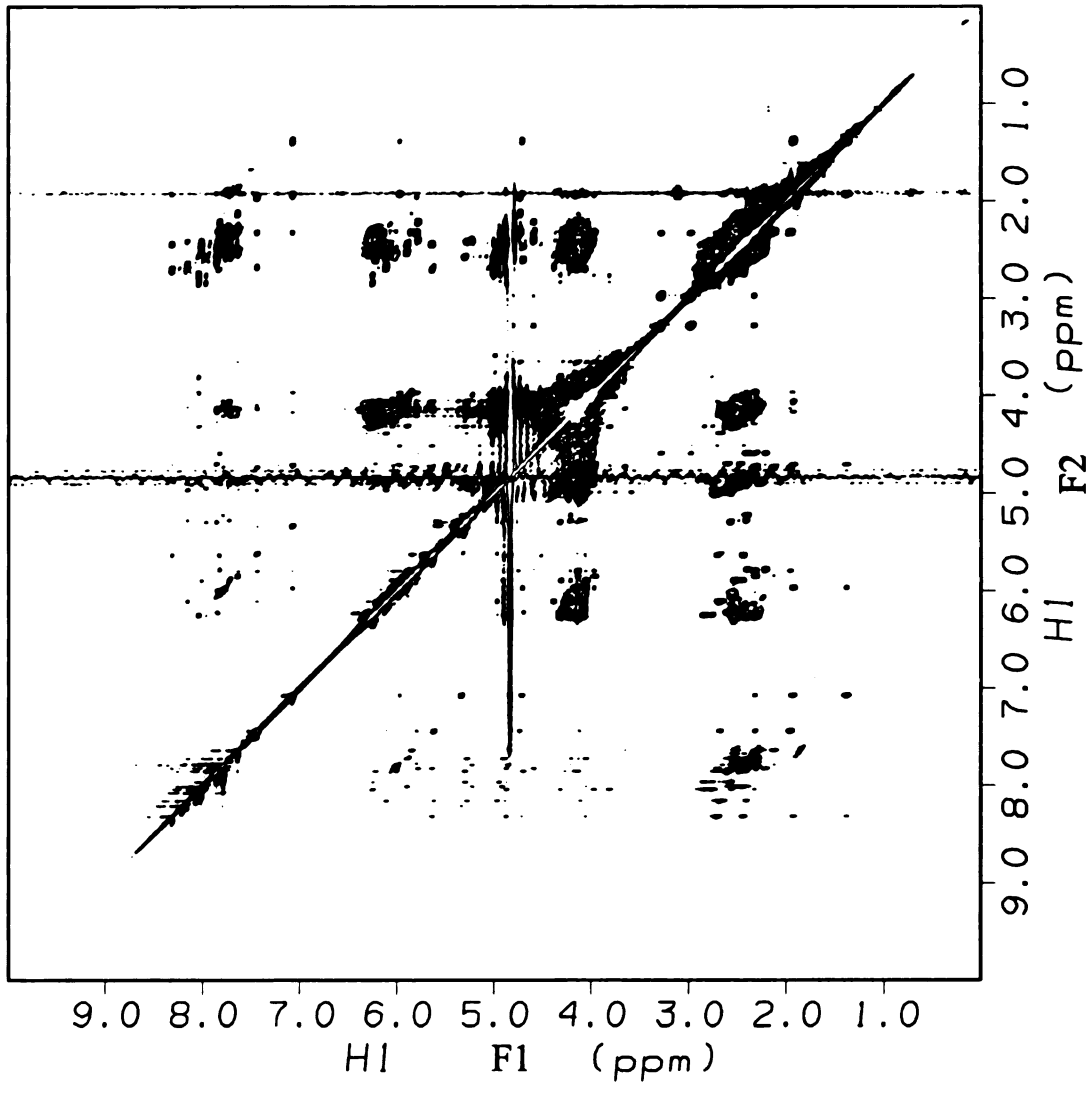

Figure 42. Rh_2-DNA Adduct NOESY Spectrum at 20 °C

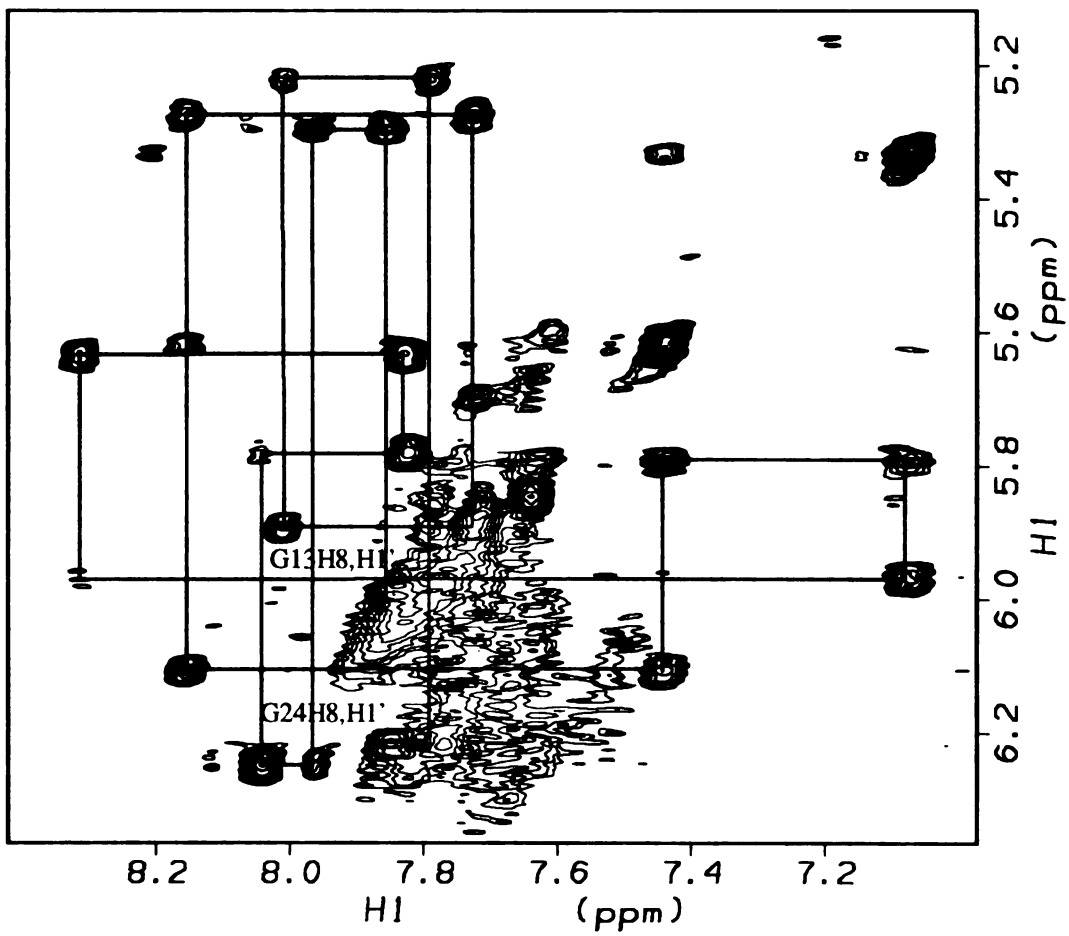

Figure 43. Base-to-H1' Region of Rh_2-DNA Adduct

frequency before returning to their original chemical shift, they will be out of phase with the spins that did not exchange. The accumulation of these phase errors over time will lead to destructive interference in the FID and loss of the signal. As a result, the FID decays rapidly and the Fourier transformation produces a broad line. This is known as exchange broadening. The greater the chemical exchange rate, the more frequently the spin visits another site with different precession frequency, and the more rapidly will be the loss of phase coherence and therefore the greater the line broadening will be.

Several attempts to overcome the severe instability of the Rh_2-DNA adduct were performed. One of the parameters that was modified to remedy this situation is temperature. Due to the fact that it was possible to obtain a NOESY walk of the H1'-to-base region of one of the strands when the temperature was lowered from 30 °C to 20 °C, it was decided to lower the temperature even further, down to 5 °C. Focusing on the same H1'-to-base region, it was observed that the breadth of the lines due to the decrease in the correlation time of the molecule at this temperature negatively affected the cross-peaks of the complimentary strand while causing only a small improvement in the resolution of resonances corresponding to the metallated strand.

A second factor that was modified is the ionic strength of the solution. By increasing the salt concentration of the sample, the negative repulsion of the phosphate backbone of the oligonucleotide is diminished. The objective is to minimize the instability of the metallated DNA as much as possible. By decreasing the electrostatic repulsion, it is possible to stabilize the adduct such that a 2D spectrum with more defined cross-peaks may be obtained.

A buffer solution of 1M Na_2HPO_4/NaH_2PO_4 (pH = 6.4) and 1M NaCl was added to the D_2O sample to obtain a final salt concentration of 50 mM Na_2HPO_4/NaH_2PO_4, 150 mM NaCl and 0.1 mM $NaC_2H_6AsO_2$ at pH = 6.5 in a final volume of 0.250 mL. It is important to note that by lowering the pH of the solution, chemical exchange may be diminished as well.

A 2D NOESY spectrum in at 5 °C was measured under these new buffer conditions. After data processing, the H1'-to-base region of the spectrum showed the cross-peaks of both strands mixed together in the same ill-defined region. We take this to mean that the degree of stability of the sample was dramatically changed to the point of causing aggregation which would lead to poor resolution of the 2D spectrum. By adding the same buffer solution to a sample in 90% H_2O, the change in stability of the sample was confirmed by observing the imino region at different temperatures (Figure 44). The breadth of the resonances increased and, as a consequence,

the signal-to-noise ratio diminished; however, the stability of the metallated duplex increased. This is clearly observed in the spectra. Even at 40 °C, some of the imino proton resonances could still be observed.

From these aforementioned experiments, it was determined that 20 °C is the best temperature for measuring the 2D NOESY spectrum. The NOESY spectrum at 20 °C, however, revealed that the molecule is quite unstable especially in the region of the metallated strand. This instability is exacerbated by the decrease in signal-to-noise ratio, which we were able to partially overcome by acquiring twice the number of scans. Unfortunatly this only increased the signal-to-noise ratio by 40 percent. For this reason, more assignments of the cross-peaks of the spectrum are not possible to make at this time.

It is evident that further manipulation of the sample is required if we are to obtain a better resolved spectrum with more dispersed cross-peaks in both dimensions. The attempts that have been made to date lead us to conclude that this will not be a straightforward task, and that additional factors such as concentration and use of buffer solutions will have to be taken into account.

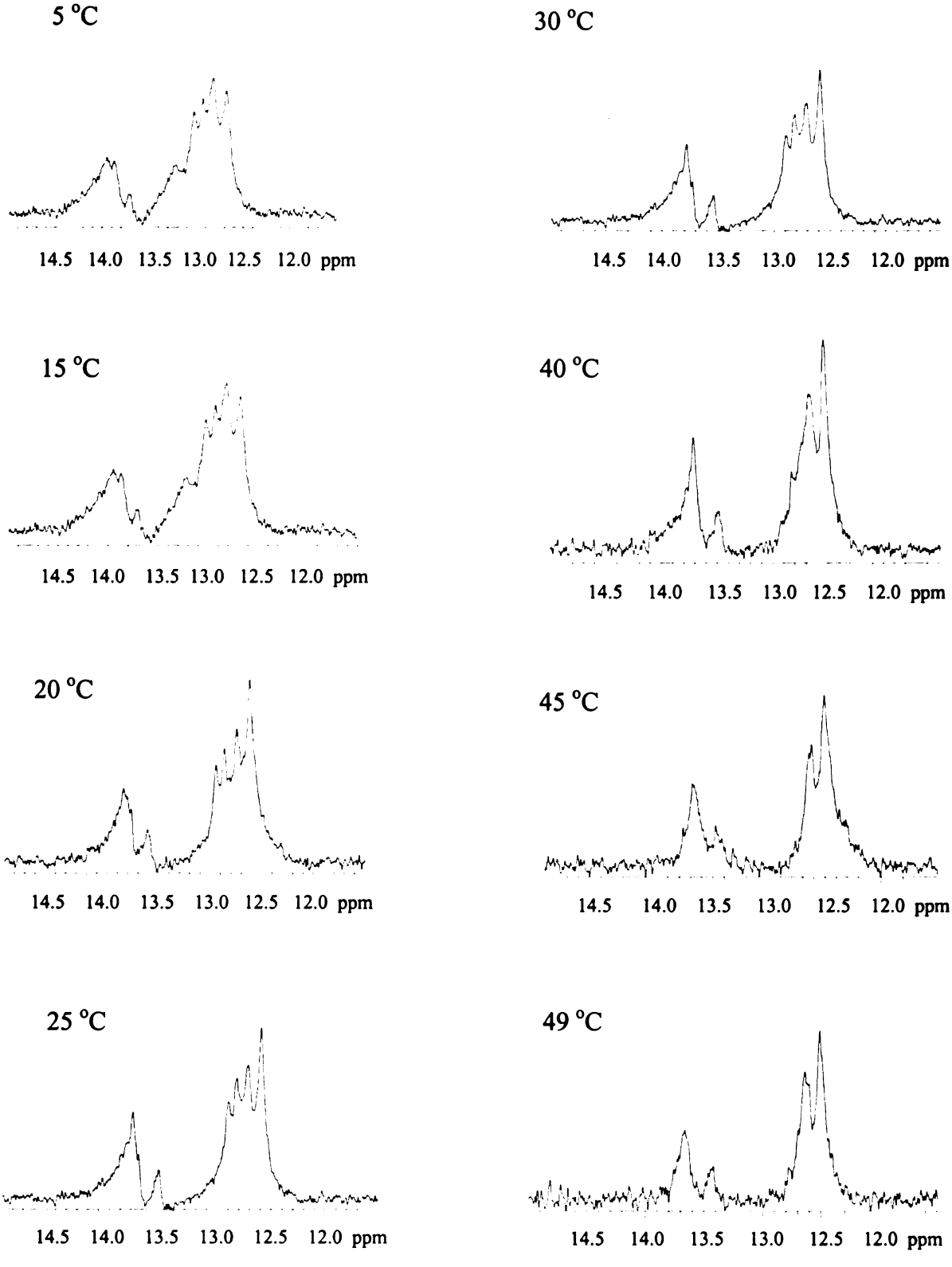

Figure 44. Imino Region of Rh_2-DNA Adduct in Buffer Solution

Chapter 4

1. MOLECULAR MODELING STUDIES

The ultimate goal of ^{1}H NMR spectroscopic measurements on large biomolecules is the modeling of structural features that will satisfy the NMR data as well as chemical information. The structure of the DNA double helix varies according to its sequence and physical environment. Internuclear distances, torsion angles, bond lengths and bond angles are characteristics of the molecule that provide important restraints for the determination of its structure. Structural determination involves taking the restraints together with the covalent structure and inputting into them a computational algorithm that searches the conformational space. This method provides a series of possible or feasible structures that satisfy the assigned structural restraints.

Determination of DNA structures by ^{1}H NMR spectroscopy is an alternative to X-ray crystallography, and also provides valuable complementary information about solution structure. The main difference between these two techniques is that in X-ray crystallography typically only one structure with a minimum energy in the solid state is obtained.

However, with NMR spectroscopy, according to the quality and number of restraints that can be extracted from the multidimensional experiments, a set of similar structures of varying energies are obtained as expected for molecules in the solution state. New techniques and computational programs are continually being developed in order to establish more accurate restraints and, consequently, to narrow the set of possible structures for the molecules.

As stated earlier, the intensity of the NOE cross-peaks is inversely related to the distance between two nuclei. Therefore, an accurate measurement of the volume of each of the cross-peaks will give rise to an array of inter-proton distance restraints. Interestingly, the two protons that give rise to a cross-peak are not alone in the molecule. They belong to a coupled network. However, assuming that each cross-peak is due to two isolated nuclear spins is a good approximation; this is referred to as the two spin or Isolated Spin Pair Approximation (ISPA) represented by the following equation:[37]

$$r_{ab} = r_{ref} (a_{ref} / a_{ab})^{1/6}$$

where r_{ab} is the interproton distance between nuclei a and b that needs to be determined, a_{ab} is the corresponding NOE cross-peak intensity and a_{ref} and a_{ab} are the known interproton distance and cross-peak intensity respectively.

The reference distances can be obtained from fixed covalent distances within the molecule under investigation. These distances can be related to the cross-peak intensities in the NOE spectrum. However, it is important to note that the mixing time (τ_m) of the NOE experiment plays a critical role in the accuracy of the NOE measurements that can be obtained. A limitation of ISPA is the omission of factors such as spin diffusion that may give rise to cross-peaks of greater intensities than those expected, which would lead to an inaccurate assessment of distances.

Structural information can be obtained by using torsion angle restraints and NOE distance restraints. To obtain data of the former, correlation spectroscopy (COSY) in any of its variations must be performed. From these experiments, measurements of coupling constants provide torsion angle restraints in the sugar deoxyribose rings [38] which consequently help to define the conformation of the DNA sugar phosphate backbone (Figure 45).

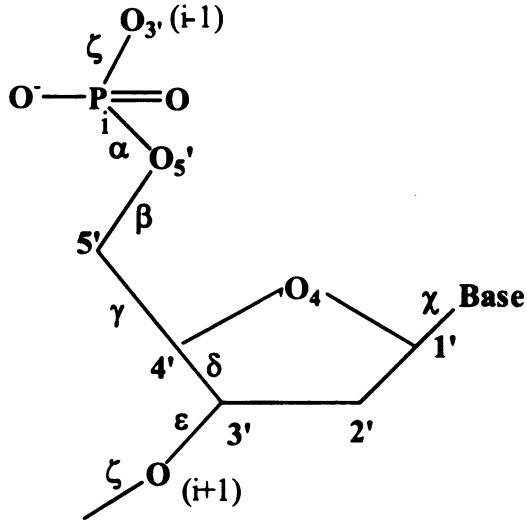

Figure 45. DNA Backbone Showing Torsion Angles

Regarding NOE distance restraints, simulated annealing (SA), which is a form of restrained molecular dynamics, relates the experimental structural restraints with energy considerations. In this approach, the potential energy is calculated for a set of atomic coordinates using a force field whose limits are determined by the values established for the restraint bounds and standard covalent bond parameters (lengths, angles). The farther the NOE distance restraints are from these bounds, the higher the potential energy of the molecule and therefore, the greater the degree of instability of the structure.

In simulated annealing, an initial structure is selected. This structure is allowed to search conformational space. After that, the set of restraints, (torsion and/or distance) is applied. These restraints will be responsible for the final structure obtained. By repeating the process several times, the structures produced at the end, although not identical, should be very similar with a small atomic root mean square deviation (RMSD) between them (<1Å). The different structures are averaged and a final structure is reported. Furthermore, several structures can be considered as initial structures, *e.g.*, A and B-type DNA, with the expectation that similar structures will be obtained if the restraint set is sufficient.

For the dodecanucleotide under study, the NOESY data obtained from the spectrum measured at 30 °C gives rise to assignments of 718 NOE cross-peaks from both sides of the diagonal. These assignments were introduced in a table under FELIX 97.0 (Molecular Simulations Inc.) which generated the volumes table that represents the intensity of each cross-peak. The reference distance and cross-peak intensity were obtained from the C19 residue, specifically, C19:H5-C19:H6 covalent bond distance (2.464 Å) and C19:H2'-C19:H2" distance (1.785 Å). From these tables, the restraints file was obtained with a total of 320 restraints calculated. Some of the restraints

were ignored due to overlapping problems that would leads to erroneous distance information.

The restraints file was exported to the structural calculation program InsightII (Molecular Simulation Inc.). Within InsightII, the simulated annealing module was selected for the refinement calculations. Together with the NOE distance restraints obtained from the NOE spectrum in D_2O, some additional restraints regarding the imino-imino cross-peaks from the NOESY spectrum in H_2O were included. To enforce proper base pairing, hydrogen bonding restraints were also used for all Watson-Crick base pairs in the sequence. The starting structure selected was the sequence in standard B form conformation. The set of restraints was displayed on this molecule and this result is presented in Figure 46.

The simulated annealing protocol contains a Molecular Dynamics schedule (MD_Schedule) edit command that provides a flexible and easy-to-use interface for designing new protocols according to the requirements of the molecule under study. For the DNA oligonucleotide, the restrained molecular dynamics protocol begins with a minimization of the B-form DNA duplex with gradual application of the restraints and the force constants by 10 percent increments. The molecule was allowed to adopt randomized velocities from the beginning of the protocol. The simulated

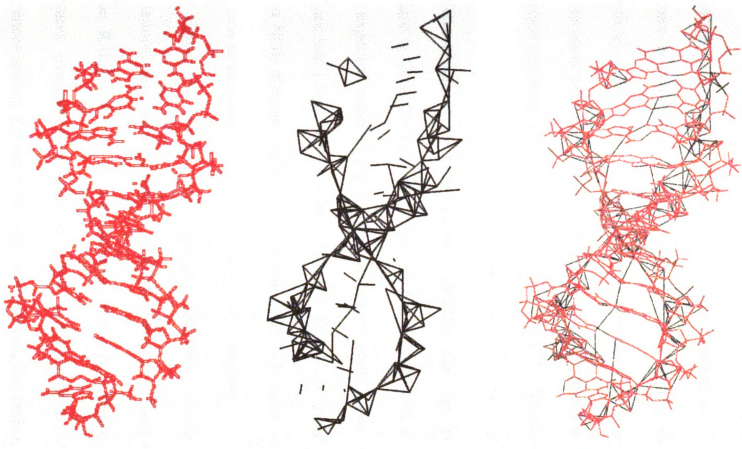

Figure 46. DNA Structure Showing NOE-Distance and Distance Restraints

annealing Quartic system applies the non-bond repulsion energy values gently. This first step in the protocol is followed by two dynamic processes starting with a steepest descent minimization algorithm. The molecular structure is heated from 0 to 300 K for 1000 ps under fully restrained conditions. The second dynamics process involves a conjugate gradient minimization algorithm that uses the cartesian coordinates of the atoms as the space variables, keeping the temperature at 300 K. These conditions led to sufficiently randomized starting geometries that, after a final conjugate gradient minimization, gave rise to a structure that lies well within the standard B-form DNA family. Some structural distortions are observed as were expected, especially at the ends of the molecule. The final structure obtained had a total energy of approximately 2202 Kcal. Energy increments due to NOE distance violations were lower than 200 Kcal comprising less than 10% of the overall energy of the molecular structure.

Figure 47 shows superimposed structures resulting from ten simulations, each starting from a different trajectory. Convergence to an atomic RMSD of 0.87 Å was achieved using this protocol. The ten structures overlapped with fairly good reproducibility. Most of the differences among the structures are observed near the ends of the duplex. This is due to the lower number of restraints in these regions of the

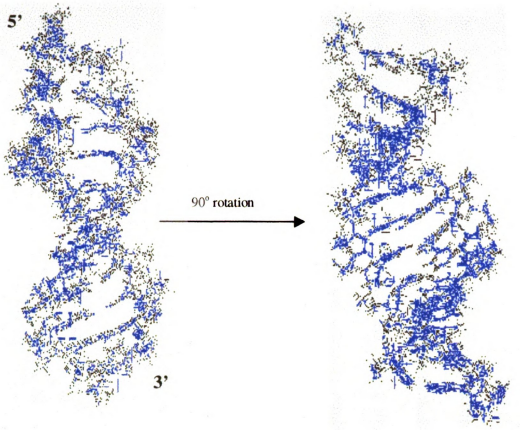

Figure 47. Superimposed Structures of d(CCTCTGGTCTCC)·d(GGAGACCAGAGG) using SA

molecule, and it reflects the greater freedom of motion in solution. It is clear that the restraints for the ends of the molecule, which are the same throughout the entire DNA duplex, are insufficient for defining the structure at the ends with the same degree of reproducibility as for the, more stable, middle part of the strand.

In conclusion, for this oligonucleotide, it was demonstrated that the assignment of the majority of the non-exchangeable protons and of some of the exchangeable protons were sufficient for the restrained molecular dynamics refinement, starting from randomized models to produce converged structures. Future studies will be directed towards the structural determination of the Rh_2-DNA adduct in solution by using this protocol.

CONCLUSIONS

Although major advances have been made regarding the mechanism of action of the anticancer drug cisplatin, the molecular aspects of metal-DNA covalent interactions are still not well understood. In the case of antitumor active dirhodium carboxylate compounds, DNA binding studies were initiated in the early 1970's, but no conclusive data were obtained. Our group has been the first to investigate the structures that these dinuclear compounds form with DNA. Regarding this matter, the work described in this thesis represents a promising first step. Structural studies of unmetallated and metallated oligonucleotides are presently being performed with good results.

^{1}H NMR spectroscopic studies of the unmetallated DNA duplex were very important to perform in order to clearly understand the behavior of the oligonucleotide in solution. Duplex stability was determined by the observation of the imino region and the type of conformation that this sequence preferentially adopts by assigning the NOE cross-peaks of the two

dimensional spectrum and further application of the NOE distance restraints to the molecule in a molecular modeling routine.

One of the most important aspects of such a study is the sequence, which, in this case, consists of one purine-rich strand and one pyrimidine-rich strand. From the base-stacking point of view, each strand exhibits a different degree of stability since the pyrimidine base stacking is not as efficient as the purine base stacking due to the absence of the imidazole ring in the former. Although this issue is not important for the stability of the unmetallated duplex, it indeed contributes to the deviations of this oligonucleotide from the standard B-form DNA. This instability, however, becomes quite evident in the metallated duplex, due to the fact that the strand directly affected by the dirhodium carboxylate compound is the one that is composed mostly of pyrimidine bases. This is most likely the reason for the high degree of instability of the DNA duplex. The correlation time measurements showed a difference between the unmetallated and metallated duplexes values of 0.8 ns. This difference implies that the Rh_2-DNA adduct molecule tumbles faster in solution. A bent conformation may be a cause of this difference, because it would allow for rapid motion. In spite of the instability, it can be concluded that after the reaction and further annealing of the complementary strand, the DNA oligonucleotide remains as a

permanent duplex as was observed in the imino region. The degree of stability of the metallated duplex however, in comparison to the native DNA duplex has decreased by about 20 °C. The formation of the Rh_2-DNA duplex demonstrated that dirhodium carboxylate compounds remain bound to double stranded DNA at different temperatures, pH and salt concentrations.

Further ^1H NMR spectroscopic studies must be accomplished in order to confirm these initial observations about the metallated sample. Sample concentration is one of the parameters that is important for determining the quality of the data. By increasing the concentration of the Rh_2-DNA adduct by 4 to 5 times, the problem of signal-to-noise ratio would be diminished which may open up the possibility for the acquisition of a better spectrum without the collection of many scans during each t_1 increment. With respect to the stability of the sample, the use of different stabilizing agents will be the next variable to alter. It is known that spermine (N,N'-bis[3-Aminopropyl]-1,4-butanediamine) is a polar molecule that is very useful for stabilization of DNA oligonucleotides in solution. The permitivity of the sample will not greatly be altered since the ionic strength of the solution will not be drastically increased as with the high salt concentration buffers used during these first experiments. Furthermore, measurements of chemical

exchange rates of the imino protons with water molecules is a straightforward experiment that will provide important information about the stability of the base pairs of the metallated duplex, especially at the site of the reaction site and adjacent base pairs nearby.

A combination of the experiments described in this thesis may allow for a two-dimensional spectrum of the quality required for further assignment and determination of the structure of the dirhodium-DNA adduct. The results will be compared to X-ray crystallographic studies that are being performed at the present time. These studies represent the initial step towards understanding, at the molecular level, the DNA binding of dinuclear antitumor agents and may help us to design more effective drugs.

LIST OF REFERENCES

LIST OF REFERENCES

1. Rosenberg, B.; Van Camp, L.; Krigas, T. *Nature*, **1965**, *205*, 698-699.

2. (a) Lim, M. C.; Martin, R. B.; *J. Inorg. Nucl. Chem.* **1976**, *38*, 1911. (b) Roberts J. J.; Thomson A. J. *Prog. Nucleic Acid Res. Molec. Biol.* **1979**, *22*, 71-133.

3. (a) Harder, H.C.; Rosenberg B.; *Int. J. Cancer*, **1970**, *6*, 207. (b) Howle, J. A.; Gale, G. R.; *Biochem. Pharmacol.* **1970**, *19*, 2757.

4. Voet, D.; Voet, J. G.; *Biochemistry*, **1990**, John Wiley & Sons. Inc.

5. (a) Bancroft, D-P.; Lepre, C.A.; Lippard S.J. *J. Am. Chem. Soc.* **1990**, *112*, 6860. (b) Fichtinger-Schepman, A. M. J.; van der Veer, J.L.; den Hartog, J. H. J.; Lohman, P. H. M.; Reedijk, J. *Biochemistry*, **1985,** *24*, 707-713. (c) Sip, M.; Schwartz, A.; Vovelle, F.; Ptak, M.; Leng, M. *Biochemistry* **1992,** *31*, 2508-2513. (d) Shwartz, A.; Leng, M. *J. Mol. Biol.* **1994,** *236*, 969-974.

6. (a) Bellon, S. F.; Coleman, J. H.; Lippard, S. J. *Biochemistry*, **1991**, *30*, 8026-8035. (b) Brabec V.; Kleinwachter V.; Butour J-L.; Johnson N. *Biophysical Chemistry*, **1990**, *35*, 129-141. (c) Rice J.A.; Crothers D. M.; Pinto A. L.; Lippard, S. J. *Proc. Natl. Acad. Sci. USA*, **1988**, *85*, 4158-4161.

7. Takahara. P.M.; Frederick, C. A.; Lippard, S. J. *J. Am. Chem. Soc.* **1996**, *118*, 12309-12321.

8. Corda, Y.; Anin M.-F.; Leng, M.; Job, D. *Biochemistry*, **1992,** *31*, 1904-1908. (b) Anderson, K.S.; *Mutat. Res.* **1979**, *67*, 209-214. (c) Bradley, L. J. N.; Yarema, K. J.; Lippard, S.J.; Essigmann, J. M. *Biochemistry*, **1993**, *32*, 982-988.

9. (a) Chao, C. C–K.; Huang, S.-L.; Lee, L-Y.; Lin-Chao, S. *Biochem. J.* **1991**, *277*, 875-880. (b) Calson, D.; Frit, D.; Salles, B. *Nucleic Acids Research*, **1992**, *20*, 6363-6368. (c) Chu, G. *J. Biol. Chem.* **1994**, *269*, 787-790. (d) Churchill, M. E. A.; Travers, A. A. *Trends Biochem. Sci.* **1994**, *19*, 185-187.

10. Grosschedl, R.; Giese, K.; Pagel, J. *Trends. Genet.* **1994**, *10*, 94-100

11. (a) Love, J.J.; Li, X.; Case, D. A.; Giese, K.; Grosschedl, R.; Wright, P.E. *Nature*, **1995**, *376*, 791-795. (b) Werner, M. H.; Huth, J. R.; Gronenborn, A. M.; Clore, G. M. *Cell*, **1995**, *81*, 705-714.

12. Takahara. P.M.; Rosenzweig, A.C.; Frederick, C. A.; Lippard, S. J. *Nature*, **1995**, *377*, 12309-12321.

13. Ohndorf U-M.; Whitehead, J. P.; Raju, N. L.; Lippard, S. J. *Biochemistry*, **1997**, *36*, 14807-14815.

14. Pasco, J. M.; Roberts, J. *J. Biochem. Pharmacol.* **1974**, *23*, 1345.

15. Ciccarelli, R. B.; Solomon, M. J.; Varshavsky, A.; Lippard, S. J. *Biochemistry*, **1985**, *24*, 7533.

16. (a) den Hartog, J. H. J.; Altona, C.; van Boom, J. H.; Marcelis, A. T. M.; van der Marel, G. A.; Rinkl L. J.; Wille-Zazeleger, G.; Reedijk, J. *Eur. J. Biochem*, **1985**, *147*, 371-379. (b) Gibson, D.; Lippard, S. J. *Inorg. Chem.* **1987**, *26*, 2275-2279.

17. Vichi, P.; Coin, F.; Renaud, J-P.; Vermeulen, W.; Hoeijmakers, J. H. J.; Moras, D.; Egly, J-M. *The EMBO Journal*, **1997**, *16*, 24, 7444.

18. (a) Hambley, T. W. *Coordination Chemistry Reviews*, **1997**, *166*, 181-223. (b) Howell, S. B., Ed.; Platinum and Other Metal Complexes in Cancer Chemotherapy Plenum Press, New York, **1991**. (c) Knox, R Friedles, F.; Lydall, D.; Roberts, J. *Cancer Res.* **1986**, *46*, 1972. (d) Blommaert, F. A.; van Kijt-Knijnenburg, H. C. M.; Dijt, F. J.; den Engelse, L.; Baan, R. A.; Berends, F.; Fichtinger-Schepman, A. M. J. *Biochemistry*, **1995**, *32*, 11676.

19. (a) Weiss, R.B.; Christian, M. C. *Drugs*, **1993**, *46*, 360. (b) Mckeage, M. J.; Morgan, S. E.; Boxall, F. E.; Hard, G. C. *Annals of Oncol.* **1992**, 111. (c) Mckeage, M. J.; Boxall, F. E.; Jones, M.; Harrap, K. R. *Canc. Res.* **1994**, *54*, 1. (d) Casazza, A. M.; Rose, W. C.; Comereske, C.; Oleson, R.; Fairchild, C. *Proc. Am. Assoc. Canc. Res.* **1992**, *33*, 536. (e) Judson, I.; Mckeage, M. J.; Raynaud, F.; Hanwell, J.; Berry, C.; Burrer, B.; Crabeels, D.; Harrap, K. Abstracts, *7th International Symposium on Platinum and Other Metal Coordination Compounds in Cancer Chemotherapy*, **1995**, 5054.

20. (a) Levi, F.; Misset, J. L.; Brienza, S.; Adam, R.; Metzger, G.; Itzakhi, M.; Caussanel, J. P.; Kunstlinger, F.; Lecouturier, S.; Descorps-Declere, A.; Jasmin, C.; Bismuth, H.; Reinberg, A. *Cancer*, **1991**, *69*, 893. (b) Extra, J. M.; Espie, M.; Calvo, F.; Ferme, C.; Mignot, L.; Marty, M. *Cancer Chemotherapy Reports*, **1990**, *25*, 299.

21. Manzotti, C.; Pezzoni, G.; Giuliani, F.; Valsecchi, M.; Farrell, N.; Tognella, S. *Proc. AACR*, **1994**, *35*, 2628.

22. Bloemink, M. J.; Reedijk, J.; Farrell, N.; Qu, Y.; Stetsenko, A. I. *J. Chem. Soc. Chem. Commun.* **1992**, 1002.

23. (a) Zou, Y.; Van Houten, B.; Farrell, N.; Biochemistry, 1994, 33, 5404. (b) Wu, P. K.; Qu, Y.; Van Houten, B.; Farrell, N. *J. Inorg. Biochem.* **1994**, *54*, 207. (c) Farrell, N.; Qu, Y.; Feng, L.; Van Houten, B. *Biochemistry*, **1990a**, *29*, 9522.

24. Johnson, A.; Qu, Y.; Van Houten, B.; Farrell, N. *Nucleic Acids Res.* **1992**, *20*, 1697.

25. (a) Bear, J. L.; Gray, H. B. Jr.; Rainen, L.; Chang, I. M.; Howard, R.; Serio, G.; Kimball, A. P. *Cancer Chemother. Rept.* **1975**, *50*, 611. (b) Bear, J. L.; Erck, A.; Sherwood, E.; Kimball, A. P. *Cancer Research*, **1976**, *36*, 2204. (c) Rainen, L.; Howard, R. A.; Kimball, A. P.; Bear, J. L. *Inorg. Chem.* **1975**, Vol 14, *11*, 2752.

26. Fimiani, V.; Ainis, T.; Cavallaro, A.; Piraino, P. *J. Chemother.* **1990**, *2*, 319.

27. Dunbar, K. R.; Matonic, J. H.; Saharan, V. P.; Crawford, C. A.; Christou, G. *J. Am. Chem. Soc.* **1994**, *116*, 2201.

28. (a) Fichtinger-Schepman, A. M. J.; van der Veer, J. L.; den Hartog, J. H. J.; Lohman, P. H. M.; Reedijk, J. *Biochemistry*, **1985**, *24*, 707. (b) Kozelka, J.; Petsko, G. A.; Lippard, S. J. *J. Am. Chem. Soc.* **1985**, *107*, 4079. (c) Sherman, S. E.; Gibson, D.; Wang, A. H-J.; Lippard, S. J. *Science*, **1985**, *230*, 412. (d) Bellon, S. F.; Coleman, J. H.; Lippard, S. J. *Biochemistry*, **1991**, *30*, 8026. (e) Van Hemelryck B.; Guittet, E.; Chottard, G.; Girault, J-P.; Huynh-Dinh, T.; Lallemand J-Y.; Igolen, J.; Chottard, J-C. *J. Am. Chem. Soc.* **1984**, *106*, 3037. (f) Berners-Price, S. J.; Ranford, J. D.; Sadler, P. *J. Inorg. Chem.* **1994**, *33*, 5842.

29. (a) den Hartog, J. H. J.; Altona, C.; van Boom, J. H.; van der Marel, G. A.; Haasnoot, D. A. G.; Reedijk, J. *J. Am. Chem. Soc.* **1984**, *106*, 1528. (b) Parnham, K.; Berners-Price, S. *Angew. Chem. Int. Ed. Engl.* **1995**, *34*, 17. (c) Huang, H.; Zhu, L.; Reid, F. R.; Drobny, G. P.; Hopkins, P. B. *Science*, **1995**, *270*, 1842. (d) den Hartog, J. H. J.; Altona, C.; van den Elst, H.; van der Marel G. A.; Reedijk, J. *Inorg. Chem.* **1985**, *24*, 986. (e) Iwamoto, M.; Mukundan, S. Jr.; Marzilli, L. G. *J. Am. Chem. Soc.* **1994**, *116*, 6238. (f) den Hartog, J. H. J.; Altona, C.; van Boom, J. H.; van der Marel, G. A.; Haasnoot, D. A. G.; Reedijk, J. *J. Biomol. Struct. Dynm.* **1985**, Vol. 2, *6*, 1137.

30. Yang, D.; van Boom, S. G. E.; Reedijk, J.; van Boom, J. H.; Wang, A. J. H. *Biochemistry*, **1995**, *34*, 12912.

31. (a) Callihan, D.; West, J.; Kumar, S.; Schweitzer, B. I.; Logan, T. M. *J. Magn. Reson.* **1996B**, *112*, 82. (b) Piotto, M.; Sandek, V.; Sklenar, V. *J. Biomol. NMR*, **1992**, *2*, 661. (c) Sklenar, V.; Piotto, M.; Leppik, R.; Sandlek, V. *J. Magn. Reson.* **1993A**, *102*, 244.

32. Bishop, K. D.; Borer, P. N.; Pelczer, I. *J. Magn. Reson.* **1996B**, *110*, 9.

33. Wuthrich, K. *NMR of Proteins and Nucleic Acids*, **1986**, John Wiley and Sons. Inc. USA

34. Suzuki, E-I.; Pattabiraman, N.; Zon, G.; James, T. L. *Biochemistry*, **1986**, *25*, 6854.

35. (a) Broido, M. S.; Zon, G.; James, T. L. *Biochem. Biophys. Res. Commun.* **1984**, *119*, 663. (b) Feigon, J.; Denny, W. A.; Leupin, W.; Kearns, D. R. *Biochemistry*, **1983**, *22*, 5930. (c) Scheek, R. M.; Russo, N.; Boelens, R.; Kaptein, R.; van Boom, J. H. *J. Am. Chem. Soc.* **1983**, *105*, 2914.

36. Croasman, W. R.; Carlson, R. M. K. *Two Dimensional NMR Spectroscopy. Applications for Chemists and Biochemists*, **1984**, VCH Publishers Inc.

37. James, T. L.; Bishop, K. D.; Blocker, F.; Gonzalez, C.; Kumar, A.; Liu, H.; Mujeeb, A.; Schmitz, U.; Ulyanov, N. B.; Yuan, Y-C.; Weisz, K. *NATO ASI Series*, **1994**, *87*, 335.

38. a) Rinkel, L. J.; Altona, C. J. Biomol. Struct. Dyn. 1987, 4, 621.
b) Weisz, K.; Shafer, R. H.; Egan, W.; James, T. L. *Biochemistry*, **1992**, *31*, 7477.